# Development of a multi-modality hydrogen delivery infrastructure: An optimization model for design and operation

*Federico Parolin, Paolo Colbertaldo*[*]*, Stefano Campanari*

Group of Energy Conversion Systems (GECOS), Department of Energy, Politecnico di Milano – Via Lambruschini 4A, 20156, Milan, Italy

## Abstract

Hydrogen deployment as an energy vector will play a crucial role in the decarbonization of the energy and industrial sectors. Its integration with the energy system requires the development of an adequate delivery infrastructure. The identification of an optimal design and operation strategy is complex due the variety of technological options in each stage of the hydrogen supply chain. This work develops a mixed-integer linear programming model to optimize the design and operation of a hydrogen infrastructure, comprising the entire supply chain from production to demand. A crucial novelty element is the combination of technical alternatives and modelling features. The proposed multi-modality formulation optimizes the transport technology at each stage, selecting between pipelines, compressed hydrogen trucks, and liquid hydrogen trucks. The pipeline and road networks are built through the model integration with a Geographic Information System, and the operation is tracked with a daily resolution, following the typical day approach. The model application looks at hydrogen employment for clean mobility in a long-term scenario in the Italian region of Sicily, assuming a demand of 1.1 million equivalent passenger cars (30% of today's stock). The resulting cost-optimal infrastructure features an average cost of delivered hydrogen of 3.81 €/kg, in line with mobility targets. The supply chain relies on the concurrent use of all transport modalities, thus showing that the multiplicity of options is a key asset in the development of a hydrogen economy.

## Keywords

Hydrogen, Infrastructure, Modelling, Multi-modality, Optimization, Hydrogen Supply Chain.

## Graphical abstract

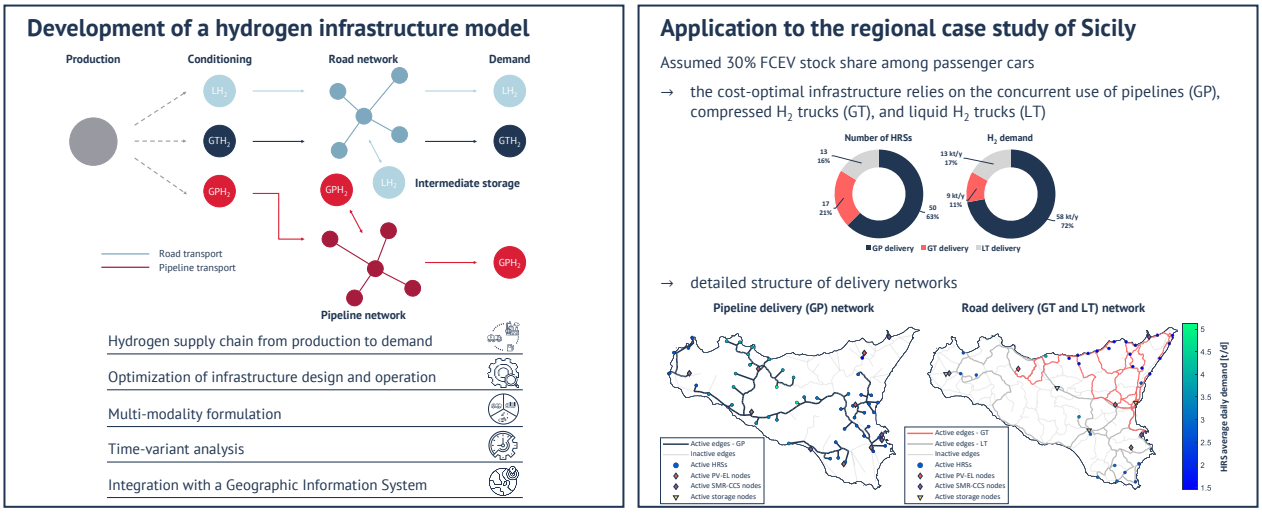


[*] Corresponding author

## Highlights

- A model for the optimal design and operation of a multi-modality hydrogen delivery infrastructure is developed.
- The modelled hydrogen supply chain comprises production, conditioning, storage, and transport up to demand nodes.
- The model optimizes the hydrogen delivery modality selecting between pipelines, gaseous trucks, and liquid trucks.
- The optimal infrastructure for long-term hydrogen mobility in Sicily reaches an average cost of hydrogen of 3.81 €/kg.
- The case study combines the three allowed transport modalities to exploit synergies.

## 1. Introduction

Driven by the increasing concern over climate change, most industrialized countries are reshaping their energy systems towards more efficient and sustainable means for generation, distribution, storage, and consumption, with the objective of a net-zero carbon balance. To achieve such an ambitious target, the involved stakeholders are required to pursue all the available strategies to abate greenhouse gas (GHG) emissions in all sectors.

Within this framework, hydrogen is expected to play a crucial role, providing a solution for long-term and large-scale energy storage and enabling sector coupling between power generation, transport, buildings, and industry. With the projected massive deployment of renewable energy sources (RES) [1], the Power-to-Hydrogen (P2H) technology is drawing increasing attention, as it allows to store renewable energy in the form of chemical energy by converting surplus electricity into hydrogen through electrolysers [2]. Different pathways can be envisaged for the produced hydrogen, as Figure 1 shows. It can be reconverted into electricity (flows *a* in the scheme) to compensate generation deficit or to provide grid balancing services. Alternatively, hydrogen in pure form can supply the demand from the transport, industrial, or residential sectors (flows *b*, *c*, and *d* in the scheme). Interest in hydrogen-powered fuel cell electric vehicles (FCEVs) has significantly increased over the last years, in which they are emerging as ideally suited for heavy-duty transport and as a promising option for passenger cars travelling long distances, since they feature a higher milage, a faster refuelling time, and a lower payload loss if compared to battery electric vehicles (BEVs). Industrial applications look at low-carbon hydrogen for the clean generation of high-grade heat or to unlock new opportunities in the production of 'green' chemicals (e.g., methanol and ammonia), in steelmaking, and in other segments where decarbonization is extremely challenging [3]. The adoption of hydrogen is also investigated to reduce the environmental impact of residential heating, as blending of hydrogen with natural gas and biomethane or the possibility to deliver pure hydrogen represent two viable options to decarbonize the natural gas grid (flows *e* in the scheme) [4]. Finally, hydrogen can be converted into other low-carbon liquid or gaseous fuels (flows *f* in the scheme) for applications where such fluids are preferred (e.g., aviation). Some of the pathways may also intersect with blue hydrogen, mostly when a direct use is foreseen [5].

Thanks to its versatility and wide range of applications and bolstered by technological and economic advancements, hydrogen has been included in policies and investment agendas of numerous governments and institutions, among which the USA, China, Japan, South Korea [6], and the European Union [7]. However, the widespread adoption of hydrogen is currently hindered by the lack of a correspondingly extensive delivery infrastructure that allows a distributed access. The development of such infrastructure involves substantial investments, making it crucial to identify cost-optimal configurations and operational strategies. For instance, investments are expected to exceed 285 G€ in Europe by 2030, comprising the installation of electrolysers and hydrogen transport and storage systems, the scale-up and connection of RES

power plants to feed the production of green hydrogen, and the retrofit of existing plants with carbon capture and storage for the production of blue hydrogen [7].

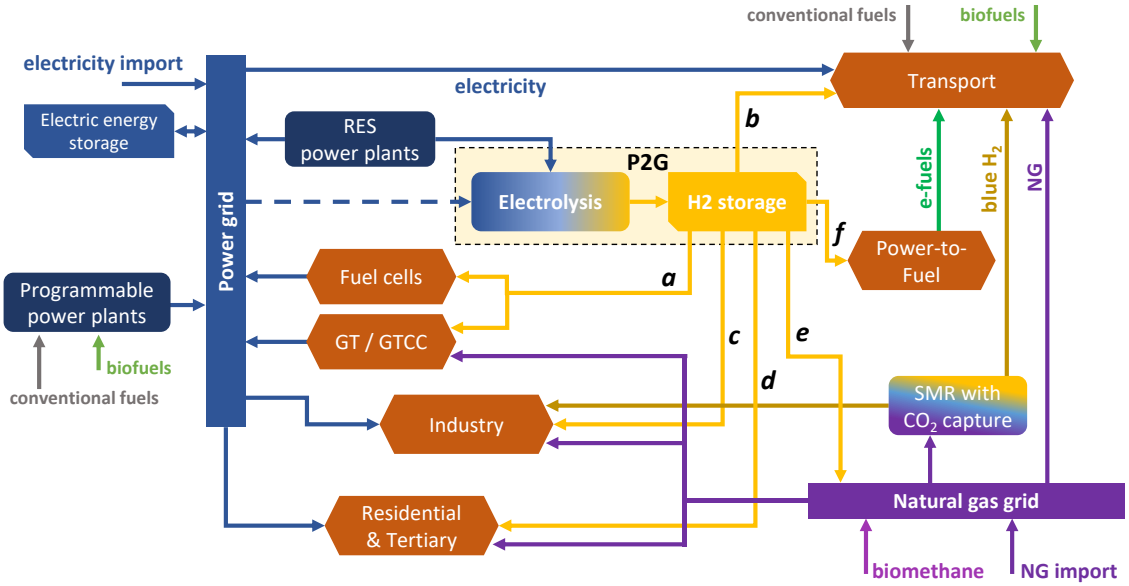


*Figure 1. Scheme of the future interwoven energy system at the nation scale, with the indication of possible hydrogen pathways.*

This work addresses the hydrogen infrastructure topic by developing a design and operation optimization model, based on mixed-integer linear programming (MILP), representing the complete hydrogen supply chain (HSC), from production sites to intermediate storage hubs and demand points, also combining multiple transport modalities. The HSC is modelled as a network of candidate nodes, where production, storage, or consumption of hydrogen may occur, and edges, along which hydrogen is transported. The network features multiple source points, characterised by different capacity limits and production profiles, which can be tailored to represent any type of production technology, either continuous/flexible or intermittent/constrained. Distinct pathways are available to connect each hydrogen source with the network of sinks and storage hubs, representing different possible transport modalities. Since pipelines and trucks rely on different infrastructures, two candidate transport networks are defined. These are built according to detailed spatial data, which are included in the model through a Geographic Information System (GIS). The proposed model formulation is general and can be applied regardless of the hydrogen end uses, e.g., industrial, civil, or mobility applications, or any mix of them. The combination of all these modelling features is a main novelty element in the topic of HSC investigation. Accordingly, model applications lead to improved insights on the infrastructure development, as well as to more accurate cost estimates.

After the model development, this work analyses, as a case study, the infrastructural needs of hydrogen-based clean mobility in a long-term scenario of the region of Sicily in Italy, in which FCEVs are widely diffused and demand points are represented by hydrogen refuelling stations (HRSs). The assessment considers the year 2050 for cost data and technological parameters and assumes a hydrogen demand equivalent to a 30% FCEV stock share among passenger cars. Since the detailed HRS management is outside the boundary of the model, the assumed hydrogen demand (80 $kt_{H2}/y$) might as well be representative of about 50% of today's heavy-duty vehicle stock converted to hydrogen fuelling [8], or of a mix of cars, trucks, buses, and trains. The transport sector is selected as hydrogen end use for the case study since it is one of the most carbon intensive sectors, accounting for more than 30% of GHG emissions in Europe [9], and HSCs for clean mobility are characterized by an interesting wide geographical span.

The remainder of the work is organized as follows. Section 2 introduces the topic of the hydrogen infrastructure, providing a general overview of the technologies and of the modelling approaches available in the literature. The adopted modelling approach and assumptions are discussed in Section 3, which lays the

ground for the analytical formulation of the model, which is presented in Section 4. Then, Section 5 outlines the analysed scenario and the employed data and parameters, while results are presented and discussed in Section 6. Finally, Section 7 summarizes the main understandings and the concluding remarks.

## 2. Technology and literature review

### 2.1. Technologies for the hydrogen supply chain

The HSC can be defined as the overall system that comprises the multiple hydrogen pathways from production to consumption, thus including production plants, storage facilities, transport routes, and demand points. The alternatives that characterize each of these stages are summarized in Figure 2 and discussed in the remainder of this section, while Section 3.2 and Section 5.3 will detail the options included in the model and the employed data, respectively.

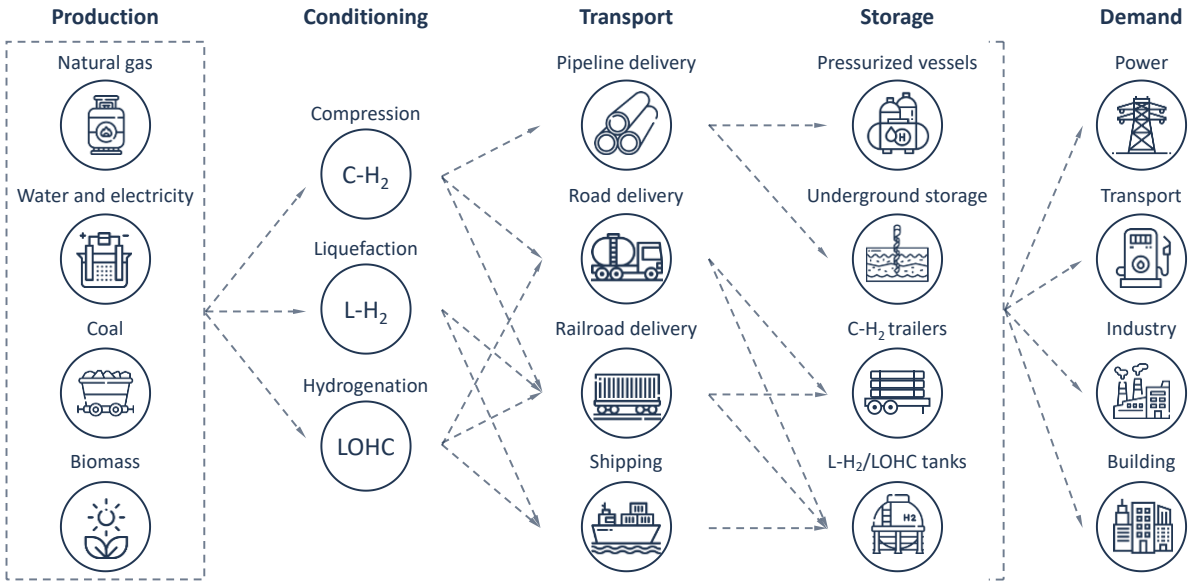


*Figure 2. Comprehensive scheme of technological options for a hydrogen supply chain.*

#### *2.1.1 Hydrogen production*

The most consolidated technologies for hydrogen production are based on fossil fuels, with natural gas accounting for about three quarters of the global supply [10]. The most widespread technology is steam methane reforming (SMR) and it is likely to remain dominant in the short term thanks to the favourable economics and the large number of facilities in operation. The levelized cost of hydrogen (LCOH) from SMR ranges between 0.7-1.5 €/$kg_{H2}$ [11], with a strong dependence on natural gas price, as capital expenditures account for only 20-25% [12]. In terms of performances, the efficiency of the process spans from 70% to 85% (LHV basis), mostly depending upon the plant size [13]. The most economically competitive process to SMR is coal gasification, which is the oldest chemical method to produce hydrogen. In this case, the efficiency is between 35-50% [13] and the production cost is in the range 1.6-2.6 €/$kg_{H2}$ [10]. Despite the economic competitiveness, the concept of hydrogen as carbon-free energy vector fails in case of production from fossil fuels, as direct $CO_2$ emissions are in the order of 7-9 $kg_{CO2}/kg_{H2}$ for SMR and of 11-19 $kg_{CO2}/kg_{H2}$ for coal gasification [10], [14]. The carbon footprint of fossil fuel-based hydrogen production can be considerably reduced by implementing carbon capture and storage (CCS) systems, where the $CO_2$ capture rate reaches or exceeds 90% at the expenses of a lower efficiency and higher CAPEX. In the case of SMR plants equipped with CCS, different facilities are already in operation and the LCOH increases to 1.6-1.9 €/$kg_{H2}$ [12], while

the adoption of CCS in coal gasification is more challenging due to the lower hydrogen-to-carbon ratio and the high level of impurities [14].

Besides fossil fuels, hydrogen can be obtained from water or biomass. Hydrogen production via water electrolysis currently accounts for only 0.1% of the global production [14], but there is significant scope for this technology to produce carbon-free hydrogen by feeding electrolysers with RES-based electricity. Over the last decade, an increase in new installations has been experienced, with a shift from pilot projects to commercial-scale systems. This enabled economies of scale that are expected to foster the cost decrease, further favouring the installations [7]. The main technologies are alkaline electrolysis (AEL), proton exchange membrane electrolysis (PEMEL), both working at low temperature (50-70 °C), and solid oxide electrolysis (SOEL), which operates at high temperature (600-900 °C) [15]. AEL is a commercial technology and features the lowest investment cost (today in the order of 750 €/$kW_e$ for multi-MW-class plants [16]) thanks to the avoidance of precious materials, but has a narrow part-load range. On the other hand, PEMEL requires expensive platinum- or iridium-based catalysts, which lead to higher specific costs on average (1000-1200 €/$kW_e$ for multi-MW-class plants) [16]. However, it offers a fast dynamic response and a wide operational range, factors that are extremely valuable when dealing with intermittent RES generation [15]. With the technological development and the increase of production volumes, costs for both AEL and PEMEL are projected to drop to 500 €/$kW_e$ by 2050 [17]–[19], while the efficiency is expected to improve, reaching an electricity consumption in the order of 45-50 $kWh_e/kg_{H2}$ [14]. Finally, SOEL offers electric efficiency values above 80%, but this technology is at a lower development stage and has not reached commercial maturity yet, entailing that a cost evolution cannot be easily foreseen [14].

Anaerobic digestion is the most mature option in hydrogen production from biomass, as it is widely diffused for biogas production. However, the process is not yet proven for high production volumes [10] and, due to the complex processing of biomass, RES-based electrolysis appears as a less expensive way to produce low-carbon hydrogen [14].

### *2.1.2 Hydrogen storage and transport*

Due to the extremely low density at ambient conditions (0.09 $kg/m^3$), hydrogen handling requires conditioning into a form that better suits transport and storage. Compressed gaseous hydrogen and liquid hydrogen represent the current state-of-the-art options.

Pressurized vessels are the most widespread solution, and today's standard is represented by Type 1 steel tanks, which allow to store gaseous hydrogen at 135-500 bar [20], [21], with costs between 355-540 €/$kg_{H2}$ [20], [22]. To further increase the pressure and, hence, the energy density, composite materials may be used. This solution is currently exploited for vehicle on-board storage, where hydrogen is stored at 350 or 700 bar [20]. In case of large-capacity storage needs, underground solutions represent an interesting option for the seasonal storage of gaseous hydrogen, benefitting from significant economies of scale. Use of existing natural gas storage facilities is under investigation, with concerns about sulphur contamination [23], whereas hydrogen storage systems in salt caverns already exist in the UK and in the USA [23], and are studied in Germany [24]. Finally, lined rock caverns (LRCs) have drawn particular attention, as they are more flexible in terms of suitable locations and geological requirements. Prototypes for natural gas have been constructed in Sweden [23] and Japan [25]; however, reliable cost and location estimates for LRCs are currently not available.

Gaseous hydrogen can be transported on land via pipeline, truck, or train. Featuring high capital expenditures and limited operational costs, pipelines are suitable for the delivery of large hydrogen amounts over long distances, up to the limit where they compete with ship transport [26], [27]. Currently, the extension of hydrogen pipelines worldwide is limited to 5000 km; most of the installations are located in the USA, Belgium, and Germany, and they are mainly employed to supply refineries and chemical facilities [14]. Compressed hydrogen trucks (also called tube trailers) consist of a trailer bed equipped with 12 to 20 steel or composite cylinders and attached to a tractor. The cylinders are filled at production sites and delivered to demand points,

where the trailer is dropped off replacing an empty one. Accordingly, partial filling and emptying is not envisaged for this option. Compressed hydrogen trucks feature moderately low capital costs and a low capacity, which make them suitable for small delivery requirements. Due to the variety of materials that can be employed and the consequent pressure levels, cost data about compressed hydrogen trucks are quite heterogeneous. Today's typical options are 400 $kg_{H2}$ metallic tube trailers with hydrogen at 200 bar and a specific capital costs of 500-600 €/$kg_{H2}$ [20], [22]. According to multiple projections [20], [22], these will be replaced by composite-based options, which offer capacities as large as 1000 $kg_{H2}$ per trailer with hydrogen at 500 bar, reaching a specific cost of 355 €/$kg_{H2}$ in the long term [22].

Liquid hydrogen is stored in cryogenic insulated tanks below the critical temperature (-240.2 °C). Thanks to the high density and the avoidance of large mechanical-resistance needs, specific costs are lower with respect to pressurized vessels, with values in the range 15-45 €/$kg_{H2}$ [20], [28]. However, due to imperfect thermal insulation, hydrogen boil-off affects this solution, which is quantified as a loss of 0.03-0.10% of the stored quantity for each day [14], [29]. Furthermore, liquefaction is an energy intensive process and its electricity consumption is significantly higher than that of compression. As an example, the electricity consumption for hydrogen compression from 30 bar (a commonly available pressure level at electrolysers and SMR outlet) to 160 bar is about 1 $kWh_e/kg_{H2}$ (assuming a compressor efficiency of 63%), whereas the current energy requirement of liquefaction is about 11 $kWh_e/kg_{H2}$, and long-term targets are in the order of 6-7 $kWh_e/kg_{H2}$ [20], [30].

Liquid hydrogen trucks (also called tanker trucks) are the transport technology for liquefied hydrogen, composed of a tractor and a trailer equipped with a single large insulated tank. Thanks to the higher density of liquid hydrogen, this option offers a larger payload and a lower specific cost if compared to compressed hydrogen trucks. Literature data about liquid hydrogen trucks are quite consistent, exhibiting specific costs in the order of 200 €/$kg_{H2}$ with capacities in the range 4000–5250 $kg_{H2}$ [14], [30], [31].

For both compressed and liquid hydrogen, railway transport is equivalent to tube trailers and tanker trucks. In analogy to liquefied natural gas tankers, liquid hydrogen can also be transported by sea in cryogenic tankers [10].

Over the recent years, liquid organic hydrogen carriers (LOHCs) have emerged as a promising alternative for hydrogen storage and transport [32]. However, the technology is still characterized by many unknowns related to scale-up and cost [14]. LOHC transport features the same options of liquid hydrogen, with the difference that these fluids can be stored at ambient temperature, thus not requiring cryogenic tanks. Accordingly, typical road tankers used for oil-based fuels can be exploited for road delivery, with a capacity of 1500-1800 $kg_{H2}$ and specific capital costs below 100 €/$kg_{H2}$ [29], [33], while existing oil tankers are available for sea transport. However, applications are limited to a few examples [34], [35], and actual costs remain uncertain.

### 2.2. Hydrogen infrastructure models

The existing literature on the topic of HSC modelling is quite heterogeneous, as each work features distinctive assumptions and approaches, addressing the complexity of different aspects. The main approaches are here presented and discussed, highlighting the most common simplifications that are introduced when modelling the HSC. The main features of the analysed references are summarized and compared in Table 1 according to the criteria that will be introduced in the discussion.

Most studies consist of optimization models and, among them, two main categories can be identified: mono- and multi-objective formulations. The former represent the majority of cases, and the objective is typically the minimization of the total network cost. Such objective is typically featured also in multi-objective models, in which the additional targets are generally related to the environmental impact [36]–[43] and/or to the safety risk [40], [42], [43]. A different approach is followed by Brey et al. [44], who introduced a second objective on the deviation from the energy targets set by the government. The works that are not based on

optimization typically deal with parametric analyses of the HSC. Reuß et al. [45], for example, computed the cost of hydrogen for different scenarios by varying the transport and storage technologies. Similar analyses are featured also in Refs. [46], [47]. Wulf et al. [48], instead, focused on the environmental footprint of the hydrogen infrastructure, performing the life cycle assessment (LCA) of three different supply chain options.

In various works, one or more stages of the HSC are excluded from the analysis to reduce the model complexity, offering a partial description of the hydrogen pathways. A common approach is to exclude last-mile delivery (i.e., the final step of the HSC, in which hydrogen is delivered to the end users, corresponding to HRSs in the case of clean mobility) and to cluster the hydrogen demand in a few hubs, thus reducing the spatial complexity of the model. However, this simplification might bias the results towards pipeline delivery, as this is favoured by the creation of large demand hubs and by the removal of the low-flow final routing of each pathway.

A crucial aspect of HSC models is how the time dependency of quantity is handled. The most common, and simplified, approach is to consider a snapshot, i.e., a steady state condition with time-invariant quantities [49]. The studied condition is usually identified as the "worst moment" throughout the year in terms of high demand and/or low production, and the network components are sized according to what should be the most stressful situation. A more precise, yet computationally demanding, approach is to consider a year-long analysis, tracking the variation of quantities according to a certain time resolution. A different approach is followed by Samsatli et al. [50], who adopted a non-uniform hierarchical time discretization, with different time layers to model investment decisions, demand variations, and system balances. Alternatively, various studies address the evolution of the HSC over a long time horizon. Such transition is described through multi-period analyses, dividing the considered time frame in periods of equal length, treated similarly to snapshots [51], allowing to model a multi-annual time horizon with few time steps. Among the different methods, the snapshot analysis is undoubtedly more convenient from a modelling perspective, as it allows to drastically reduce the model complexity by cutting the number of variables and constraints. However, it fails to track the optimal introduction and usage of storage units [52], as they are often sized according to exogenous parameters, as, for example, by setting the capacity equal to a certain multiple of the daily hydrogen production [29], [31], [45].

Wide differences are observed regarding the spatial modelling of the HSC. Many authors follow the simplified approach of considering extremely schematized networks, thus ignoring the territorial constraints of the region. A more accurate method is to rely on a Geographic Information System (GIS) to define the candidate infrastructure network on the basis of detailed spatial data, which, however, may lead to computationally heavy models. Different examples of GIS integrations can be found in the literature. In Table 1, the integration is highlighted only for works in which GIS data are used to build the candidate hydrogen transport pathways, as this is the case that most affects the spatial complexity of the HSC.

A key challenge in modelling hydrogen transport is to include the multiplicity of delivery modes, which requires a formulation that optimizes also the selection of the transport technology for each stage of the supply chain. In most studies, even though multiple transport modalities are considered, such selection is imposed, and each analysis assumes a single modality. Despite simplifying the formulation, this method may result in a sub-optimal design of the HSC, since the optimal configuration could rely on the parallel use of multiple transport modalities. The multi-modality formulation substantially increases the level of complexity of the model, introducing additional variables and constraints. Accordingly, works that adopt such formulation typically feature simplifying assumptions in other aspects of the model, for instance, considering coarser time resolutions and/or reducing the spatial complexity by excluding last-mile delivery from the HSC description or by employing schematized networks.

As Table 1 shows, this work aims at filling the gaps in HSC modelling by integrating multiple levels of analysis. The main novelty aspect of the developed model lies in the simultaneous capabilities of including all stages of the supply chain, considering a multi-modality formulation, tracking the time variation of quantities, and integrating GIS data to build the transport networks.

*Table 1. Hydrogen delivery models review.*

| Ref. | Optimization | Prod. | Storage | Transp. | Last-mile delivery | Multi-mode | Timescale | GIS integration |
|---|---|---|---|---|---|---|---|---|
| [30] | Mono | | ✓ | ✓ | ✓ | | Snapshot | |
| [53] | Mono | ✓ | | ✓ | ✓ | | Snapshot | ✓ |
| [54] | Mono | ✓ | | ✓ | ✓ | | Snapshot | ✓ |
| [55] | Mono | ✓ | ✓ | ✓ | | ✓ | Snapshot | |
| [50] | Mono | ✓ | ✓ | ✓ | | | Time layers | |
| [56] | Mono | ✓ | | ✓ | | | Multi-period | ✓ |
| [45] | No | ✓ | ✓ | ✓ | ✓ | | Snapshot | ✓ |
| [46] | No | | ✓ | ✓ | ✓ | | Snapshot | |
| [57] | Tri | ✓ | ✓ | ✓ | | ✓ | Snapshot | |
| [48] | No | ✓ | ✓ | ✓ | ✓ | | Snapshot | |
| [36] | Bi | ✓ | ✓ | ✓ | | ✓ | Multi-period | |
| [37] | Bi | ✓ | | ✓ | | ✓ | Multi-period | |
| [38] | Bi | ✓ | | ✓ | | ✓ | Multi-period | |
| [28] | Mono | ✓ | ✓ | ✓ | ✓ | ✓ | Multi-period | |
| [39] | Bi | ✓ | | ✓ | | | Multi-period | |
| [40] | Tri | ✓ | ✓ | ✓ | ✓ | | Multi-period | ✓ |
| [58] | Mono | ✓ | ✓ | ✓ | ✓ | | Multi-period | |
| [59] | Mono | ✓ | | ✓ | ✓ | | Multi-period | ✓ |
| [18] | Mono | ✓ | | ✓ | ✓ | ✓ | Snapshot | |
| [60] | Mono | ✓ | ✓ | ✓ | ✓ | ✓ | Multi-period | |
| [44] | Bi | ✓ | | | | | Multi-period | |
| [47] | No opt. | ✓ | ✓ | ✓ | ✓ | | Snapshot | ✓ |
| [61] | Mono | ✓ | ✓ | ✓ | | ✓ | Snapshot | |
| [62] | Mono | ✓ | | | | | Snapshot | |
| [41] | Bi | ✓ | ✓ | ✓ | | ✓ | Multi-period | |
| [42] | Tri | ✓ | ✓ | ✓ | | ✓ | Snapshot | |
| [63] | Mono | ✓ | ✓ | ✓ | | ✓ | Multi-period | |
| [64] | Mono | ✓ | ✓ | ✓ | | | Snapshot | |
| [65] | Mono | ✓ | ✓ | | | | Year-long (monthly res.) | |
| [17] | Mono | ✓ | ✓ | ✓ | | | Year-long (hourly res.) | ✓ |
| [66] | Mono | ✓ | ✓ | ✓ | ✓ | ✓ | Multi-period | |
| [67] | Mono | ✓ | | ✓ | | ✓ | Long time horizon | ✓ |
| [43] | Tri | ✓ | ✓ | ✓ | | | Multi-period | |
| [31] | Mono | ✓ | ✓ | ✓ | ✓ | | Snapshot | ✓ |
| This study | Mono | ✓ | ✓ | ✓ | ✓ | ✓ | Year-long (daily res.) | ✓ |

## 3. Problem statement

This work aims at developing a model to identify the cost-optimal configuration of a HSC for a given spatial domain and a given hydrogen demand distribution, including both the design and the operational strategy of the infrastructure. The former includes the installed production and storage capacities, and the

technologies exploited to produce, store, and transport hydrogen, while the latter involves all energy and hydrogen flows that characterize the operation of the facilities over a year-long time frame.

### 3.1. Research objective

The proposed model minimizes the total annual cost of the HSC. In particular, the objective function is defined as the average cost of hydrogen delivered to demand points, which includes the expenditures related to production, storage, and transport.

The model implements a mono-objective structure, since, on the one hand, factors related to safety and financial risks were not of interest in the present work, and, on the other hand, environmental concerns are anyhow included in the model, as a carbon tax is present and therefore affects the costs in the objective function.

The HSC optimization problem is summarized as follows. The required input data are:

- the set of available hydrogen production, storage, and transport technologies, with their techno-economic data;
- the topologies of the candidate transport networks for the included transport modalities;
- the candidate locations of production sites and intermediate storage hubs;
- the locations and demand profiles of demand nodes;
- the upper boundaries for the installed production capacity;
- the electricity generation profiles in the case of RES-based hydrogen production;
- the upper boundaries for the installed storage capacity.

The model outputs the optimal configuration of the HSC, according to the input data, determining:

- the employed production, transport, and storage technologies;
- the installed production and storage capacities;
- the structure of the transport networks, the exploited pathways, and the delivered quantities;
- the operation strategy of each component of the infrastructure.

### 3.2. HSC modelling assumptions

The proposed model includes the complete hydrogen pathway from production to consumption, and the HSC comprises all the five stages reported in Figure 2. As a preliminary simplification, a subset of technologies is selected among the numerous alternatives discussed in Section 2, considering those that best suit the analysed scenario. The set of included technologies is summarized in Figure 3, and the underlying modelling assumptions are discussed in this section.

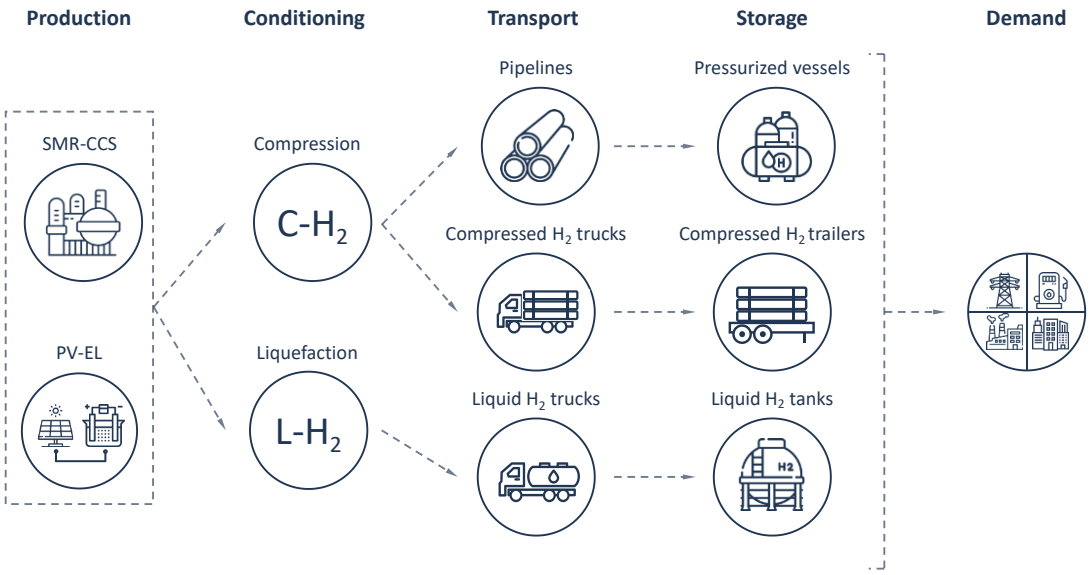


*Figure 3. Scheme of HSC technologies included in the model.*

### *3.2.1 Hydrogen production*

The model considers two main production categories: continuous/flexible or intermittent/constrained. The former includes the technologies that can operate flexibly within the installed capacity, such as SMR and coal or biomass gasification. RES-based electrolysis, instead, belongs to the second category, as hydrogen production is constrained by the availability of RES electricity, which features an intermittent generation profile.

The model implements one production type for each category: SMR equipped with CCS (SMR-CCS) as continuous/flexible and PV-fed electrolysis systems (PV-EL) as intermittent/constrained. Other production options could be included with analogous modelling approaches, but are not considered for simplicity in this work.

SMR-CCS benefits from a relatively low production cost and emission factor, thus complying with the concept of low-carbon hydrogen (see Table 2 and Table 3). As a reasonable possibility for future deployments, this work considers SMR-CCS located at existing refinery facilities, assuming that a fraction of today's hydrogen production capacity will be available for export in future due to the decrease in internal use caused by reduced demand for petrochemical products. In the analysis, electrolysis is linked to power generation from solar PV to ensure a fully-decarbonized hydrogen production. However, PV-EL systems are not assumed as stand-alone plants and integration with grid electricity is allowed to increase the electrolysis operation. Also, revenues can be obtained from the sale of surplus electricity generation (see Appendix 1 for further details on the PV-electrolysis match). Regardless of the exploited technology, production facilities include a certain storage capacity that acts as buffer between production and delivery, according to the modalities discussed in Section 3.2.2.

### *3.2.2 Hydrogen processing, storage, and delivery*

Hydrogen conditioning is assumed to take place at production sites, starting from a pressure of 30 bar, as available at both electrolysis and SMR outlet. The model assumes that hydrogen can be either compressed or liquefied, coherently with the subsequent storage and transport methods. A single production facility may host multiple conditioning systems.

Compressed hydrogen storage adopts Type 1 pressurized vessels at ambient temperature, while liquid hydrogen is stored in cryogenic tanks at atmospheric pressure. The boil-off effect is modelled as a daily percentage loss of the stored quantity (0.1 %/day).

Hydrogen is delivered to demand points or storage hubs in either gaseous or liquid form via pipelines (gaseous pipeline, GP) or trucks (gaseous truck, GT, or liquid truck, LT), consistently with conditioning. The selection of the transport modality is optimized for each stage of the supply chain, given that each demand point may treat only one mode.

For GP delivery, the installation of an entirely new pipeline network is considered. Although reconversion of the existing natural gas grid is possible [68], at least partially, this would require a separate analysis to assess the timeframe and sequence of variations, assessing the feasibility on a case-by-case basis [14]. Hydrogen pipelines are assumed to be sized between a minimum and maximum diameter, which are set to 5 cm and 50 cm, respectively, corresponding to common literature values [50], [69]. Since the pressure along pipelines is likely in the range of 100 bar, additional compression is required at intermediate storage hubs and destination points, which operate at higher pressure.

Compressed hydrogen trucks and liquid hydrogen trucks are assumed to supply a single demand point or storage hub during each trip, where they completely release their payload before returning to the starting point. While this hypothesis corresponds to the actual operation of compressed hydrogen trucks, whose trailers are dropped at the receiving points in exchange for empty ones, it is an approximation for liquid hydrogen trucks, which could supply two or more demand points along one multi-stop trip with partial deliveries. Nevertheless, the assumption allows to simplify the model and is adequate for medium-long term scenarios, considering that the consumption of demand points is projected to increase.

For both road transport modalities, a kilometric cost is considered to account for fuel consumption, driver's salary, and tractor rental cost; instead, cylinder- or tank-equipped trailers are accounted for as a purchase cost. Storage at intermediate hubs is not envisaged for compressed hydrogen trucks, which typically move straight from the production site to the drop off at the receiving point.

#### *3.2.3 Hydrogen consumption*

Demand points in the model represent final use sites with a known consumption profile. This allows to develop a general formulation that can describe scenarios with different hydrogen end uses. Accordingly, as Figure 3 shows, the same model formulation can be applied to assess the infrastructural needs arising from the use of hydrogen in heterogeneous sectors (e.g., power, transport, industry, buildings, or others). In the case of hydrogen supply to mobility, demand points represent hydrogen refuelling stations and the consumption profile is that of the station (i.e., a certain average daily hydrogen output), without the need to detail the vehicle flows and/or the internal management of compression devices.

Hence, demand is an exogenous input, provided to the model as a combination of site locations and time profiles for each location, according to the investigated application. Furthermore, it is assumed that each demand node can be supplied by only one transport modality, considering that each site will be equipped with one technology.

### 3.3. Model structure

The superstructure of the HSC model is schematized in Figure 4. In the proposed network topology, a generic node $n$ can belong to one of the following sets:

- the set of transit nodes ($n \in N_t^m$), which shape the candidate transport networks but do not contribute to production, consumption, nor storage of hydrogen;
- the set of candidate production nodes ($n \in N_p$), which represent the possible sources of hydrogen in the network and comprise conditioning facilities;

- the set of candidate intermediate storage nodes ($n \in N_s^m$), which can collect hydrogen from multiple production facilities to absorb the seasonality of production and demand;
- the set of demand nodes ($n \in N_d$), or sinks, whose nature and requirements vary according to the investigated scenario (i.e., end use).

As Figure 4 shows, road and pipeline transport occur on two distinct candidate networks, featuring different candidate transit and intermediate storage nodes, whereas production and demand nodes are unique and shared between the two networks. The produced hydrogen is injected in the respective grid through conditioning, after which variables are divided onto the two networks. Two distinct conditioning processes are considered for pipeline and compressed hydrogen truck delivery, as the pressure levels are different for the two options. Finally, hydrogen is delivered to demand nodes, each of which can be supplied via only one modality.

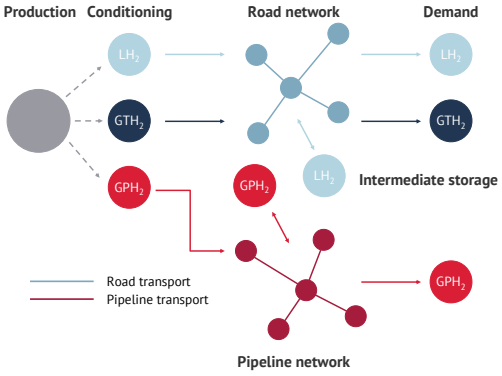


*Figure 4. Representation of the HSC pathways as structured in the model ($GPH_2$ = gaseous hydrogen via pipelines, $GTH_2$ = compressed gaseous hydrogen via truck, $LH_2$ = liquid hydrogen via truck).*

### *3.3.1 Georeferenced spatial methodology*

The hydrogen supply chain is affected in all its stages by spatial and geographical constraints. As an example, the deployment of a new pipeline network must comply with the territory morphological features and the existing road infrastructure sets the available pathways for truck delivery. Moreover, the position and distribution of hydrogen sources and sinks strongly affect the selection of the transport modality, as large and distant hubs favour pipelines, whereas a network of close demand points is more likely to call for road delivery.

In this work, a georeferenced model of the HSC is developed by building the candidate transport networks from GIS spatial data, available in the *shapefile* format [70]. Under the hypothesis that the existing road network is not saturated, truck routes are assumed to run along the existing main roads and highways. On the other hand, the development of a hydrogen pipeline network requires hypotheses on the routes where new structures can be realized, preventing them from crossing forbidden or implausible areas. Accordingly, it is assumed that pipelines could be installed following the pathway of the existing natural gas grid, which allows to identify areas where a right-of-way already exists [67]. More details about the implemented GIS methodology are given in Appendix 2.

### *3.3.2 Time scale*

To properly model the HSC, seasonal fluctuations of hydrogen production and demand must be taken into account, and the time dependency of the quantities must be considered. This becomes of paramount importance to accurately size storage facilities when RES-based hydrogen production is included.

The model is based on a time-dependent analysis considering a year-long time frame, as opposed to the most common option of snapshots. As a compromise between the level of detail and the computational complexity,

the adopted time resolution is daily (e.g., hydrogen flows are expressed in metric tonnes per day). Hence, a parameter $\widetilde{\Delta t}$ is defined to represent the time resolution of the model (1 day), as it will be relevant in the storage content evolution equations. To limit the number of variables, the year is represented as the repetition of groups of typical days, each representative of a certain period of the year. More specifically, a typical day is associated to each time step $t \in T$ and repeated $\widetilde{N}_{td}$ times, adopting an even duration of the periods. Each typical day is characterized by a hydrogen demand at each demand node and a PV generation hourly profile at each electrolysis production node (see Appendix 1). In this analysis, 52 typical days are identified (thus, the cardinality of the set $|T| = 52$), and each of them is repeated $\widetilde{N}_{td} = 7$ times to obtain the 52 weeks that constitute the year.

The advantage of the typical day approach is that it allows to maintain a daily resolution while considering only 52 time steps instead of 365 to model a year. While this type of method has been limitedly exploited in the modelling of the hydrogen supply chain (among the studies included in the survey, only by Welder et al. [17]), it is commonly used in energy systems modelling, as in Refs. [71]–[73].

## 4. Model formulation

This section illustrates the analytical formulation of the HSC model, presenting the objective function and the main equations that describe the system features and interactions, which act as constraints of the optimization problem. The entire list of symbols is detailed in the Nomenclature Section. To allow for easier reading, input parameters are distinguished from optimization variables by means of a tilde (~).

The developed model follows a MILP formulation, which ensures global optimality and is especially suitable for large-scale and highly interconnected problems such as the HSC, at the expenses of requiring adequate simplification or linearization methods to deal with common non-linearities such as economies of scale.

In the proposed formulation, at a certain time step $t \in T$, hydrogen can be produced at a production node $n \in N_p$, exploiting the technology $p \in P = \{SMR\text{-}CCS, PV\text{-}EL\}$. The produced quantity is conditioned and delivered via a transport modality $m \in M = \{GP, GT, LT\}$ to either an intermediate storage node $n \in N_s^m$ or a demand node $n \in N_d$, passing by a number of edges $e \in E^m$ and transit nodes $n \in N_t^m$. Depending on the transport modality, hydrogen can be stored exploiting the storage technology $s \in S = \{G, GT, L\}$. In general, multiple storage options can correspond to a single transport modality $m$, as, for example, hydrogen delivered via pipeline could be stored either in pressurized vessels or in underground facilities. Accordingly, transport and storage modalities are identified with the distinct indices $m$ and $s$. However, to reduce the complexity, the present work assumes that hydrogen delivered through a modality $m$ can be stored exclusively with one storage technology $s^m$. Consequently, equations refer only to the transport modality $m$, as it implicitly identifies also the related storage technology $s^m$.

Hydrogen transport occurs on separated directed graphs, each characterized by a different incidence matrix $\tilde{Y}^m$, as well as by a distinct set of edges $E^m$, of transit nodes $N_t^m$, and of candidate storage nodes $N_s^m$. To highlight the dependence of these parameters on the graphs, they are represented with the superscript $m \in M$. In the present analysis, these elements coincide for $m = GT$ and $m = LT$, as road delivery modalities share the same candidate transport network (i.e., the existing road infrastructure).

### 4.1. Objective function

The HSC model aims at minimizing the average specific cost of hydrogen delivered to demand nodes, considering the capital and operational expenditures of all the infrastructure components. Accordingly, the average cost of hydrogen (COH) is computed as the total annual cost (TAC), divided by the total annual hydrogen consumption in the network:

$$COH_{avg} = \frac{\sum_i CAPEX_i \cdot \widetilde{CRF_i} + \sum_i OPEX_i}{\sum_{n\epsilon N_d} \sum_t \tilde{q}_{dem}^{n,t} \cdot \widetilde{\Delta t} \cdot \widetilde{N}_{td}} \tag{1}$$

The capital expenditure of the generic HSC component $i$ is computed from the installed capacity and the specific capital cost in all the nodes that may include that technology:

$$CAPEX_i = \sum_{n\epsilon N_p \cup N_s^m \cup N_d} C_i^n \cdot \widetilde{capex}_i \tag{2}$$

Exceptions to Eq. (2) are the capital costs of liquefaction and pipeline installation. Liquefaction capital costs feature significant economies of scale, with a scale factor of 0.57-0.66 [29], [30]. This could be introduced via a piecewise linearization. However, it would strongly impact the computational performance due to the additional binary variables. Hence, a single-trait linearization is adopted, considering a limited capacity range, consistently with realistic installations, following a similar approach to Ref. [30]:

$$CAPEX_{LIQ} = \sum_{n\epsilon N_p} \left( \widetilde{capex}_{var,LIQ} \cdot C_{cnd}^{n,LT} + \widetilde{capex}_{fix,LIQ} \cdot \chi_{LIQ}^n \right) \tag{3}$$

Pipelines costs depend on multiple factors, such as installation, materials, rights of way, location, and topographic features. A common practice is to express CAPEX as a function of the pipeline diameter [28]–[30], [47], [53], [54]. Considering a quadratic relation between diameter and CAPEX [30], the investment cost can be expressed as a linear function of the pipeline section (treated as the "capacity" of the pipeline), taking into account the edge length $\tilde{l}^e$:

$$CAPEX_{GP} = \sum_{e\epsilon E^{GP}} \left( \widetilde{capex}_{var,GP} \cdot C_{GP}^e + \widetilde{capex}_{fix,GP} \cdot \chi_{GP}^e \right) \cdot \tilde{l}^e \tag{4}$$

Both the liquefaction capacities and the pipeline diameters are bounded by a maximum and a non-null minimum value, requiring the use of disjunctive big-M constraints [74] via the introduction of the binary variables $\chi_{LIQ}^n$ and $\chi_{GP}^e$.

Operational expenditures comprise fixed and variable costs:

$$\sum_i OPEX_i = \sum_i FC_i + \sum_i VC_i \tag{5}$$

Fixed costs account for O&M expenditures and are expressed as a percentage of CAPEX for each HSC component:

$$FC_i = \sum_i \widetilde{opex\%}_{O\&M_i} \cdot CAPEX_i \tag{6}$$

Variable costs consist of production, conditioning, road delivery, and carbon tax expenditures, as shown in Eqs. (7)-(10). The revenues from the sale of surplus electricity are considered as a negative cost in the production contribution.

$$VC_{prd} = \sum_{n\epsilon N_p} \sum_{t\epsilon T} \left( \widetilde{LCOH}_{SMR\text{-}CCS} \cdot q_{prd}^{n,SMR\text{-}CCS,t} + \tilde{c}_E \cdot E_{grid}^{n,t} - \tilde{p}_E \cdot E_{sur}^{n,t} \right) \cdot \widetilde{\Delta t} \cdot \widetilde{N}_{td} \tag{7}$$

$$VC_{cnd} = \sum_{n\epsilon N_p \cup N_s^m \cup N_d} \sum_{m\epsilon M} \sum_{t\epsilon T} \tilde{c}_E \cdot \widetilde{cons}_{cnd}^m \cdot q_{cnd}^{n,m,t} \cdot \widetilde{\Delta t} \cdot \widetilde{N}_{td} \tag{8}$$

$$VC_{RD} = \sum_{m=GT,LT} \sum_{e\epsilon E^{GT,LT}} \sum_{t\epsilon T} 2 \cdot \tilde{c}_{RD} \cdot \tilde{l}^e \cdot N_{truck}^{e,m,t} \cdot \widetilde{\Delta t} \cdot \widetilde{N}_{td} \tag{9}$$

$$VC_{CT} = \sum_{n\epsilon N_p \cup N_s^m \cup N_d} \sum_{m\epsilon M} \sum_{t\epsilon T} \tilde{c}_{tax} \left( \tilde{e}_{SMR\text{-}CCS}\, q_{prd}^{n,SMR\text{-}CCS,t} + \tilde{e}_{E,cnd}\, \widetilde{cons}_{cnd}^m\, q_{cnd}^{n,m,t} + \tilde{e}_{E,EL} E_{grid}^{n,t} \right) \widetilde{\Delta t}\, \widetilde{N}_{td} \tag{10}$$

## 4.2. Constraints

The infrastructure nodes are categorized into four types according to their role in the HSC, as schematized in Figure 5. Except for transit nodes, each node type features a storage section and a virtual sub-node, which manages the connection to other nodes of the graphs.

The following sub-sections detail the main equations implemented as model constraints to describe the HSC stages. The straightforward equations that bound the energy and mass flows within the installed capacities of the related components are not detailed. The installed capacities are decision variables and might be exogenously limited, according to the specific case study.

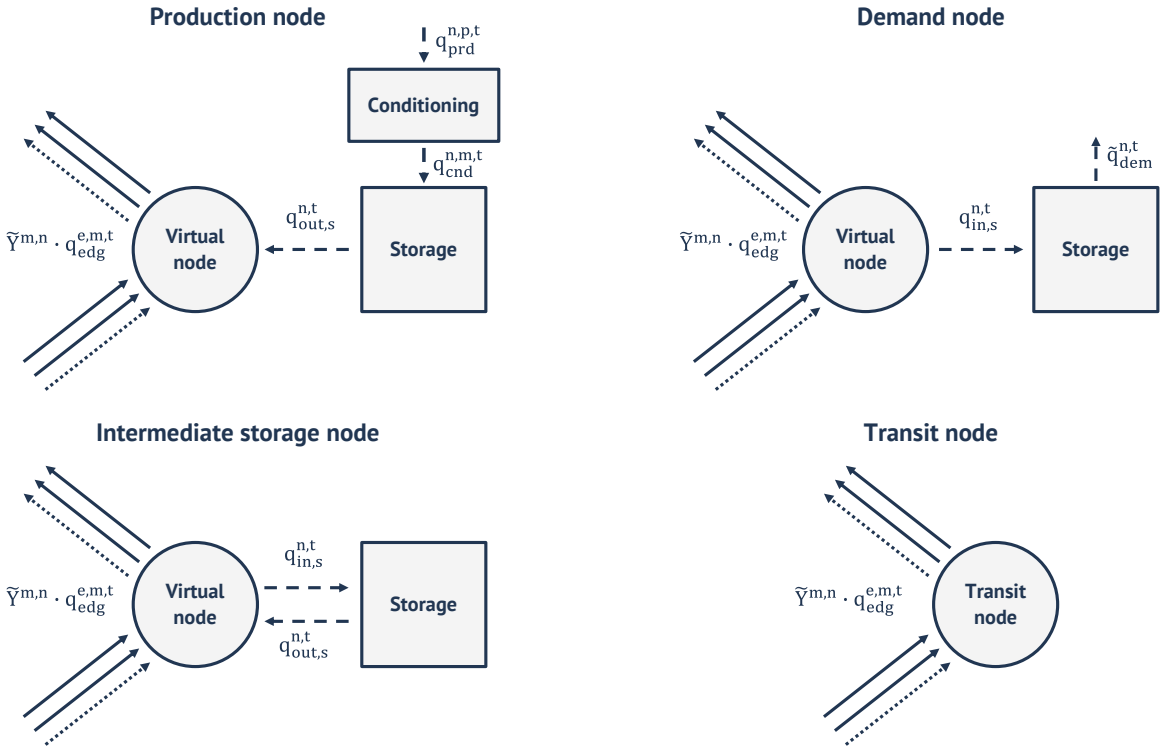


*Figure 5. Node modelling.*

### 4.2.1 *Production facilities*

For each production node, the installed production capacity ($C_{prd}^{n,p}$) is bounded by an exogenous maximum value that depends on the technology exploited and on the location of the site. For SMR-CCS production, the limit is expressed as daily hydrogen output. For PV-EL systems, the optimization variable is the nominal capacity of the PV plant ($C_{PV}^{n}$), and the nominal hydrogen production capacity ($t_{H2}$/d) is derived considering a constant ratio between PV and electrolysis capacities.

The operation of SMR-CCS and PV-EL plants is substantially different. The former can operate flexibly within the upper bound of the installed capacity (Eq. (11)), whereas the electrolysis output is constrained by the PV generation profiles (Eqs. (12)-(15)). A limited degree of flexibility is provided by the possibility to absorb grid electricity, which, however, introduces additional costs. The parameters $\tilde{f}_{PV,tot}^{n,t}$ and $\tilde{f}_{PV\text{-}EL}^{n,t}$ represent the daily generation of electricity from PV and the daily amount that could be exploited by electrolysis, respectively, per unit of PV capacity ($kWh_e/d/kW_{p,PV}$), taking into account the hourly variations and the capacity ratio $\tilde{r}_{PV\text{-}EL}$. Details are provided in Appendix 1.

$$\forall\, t, n \in N_p \qquad 0 \leq q_{prd}^{n,SMR\text{-}CCS,t} \leq C_{prd}^{n,SMR\text{-}CCS} \tag{11}$$

$$\forall\, t, n \in N_p \qquad E_{PV,tot}^{n,t} = C_{PV}^{n} \cdot \tilde{f}_{PV,tot}^{n,t} \tag{12}$$

$$\forall\, t, n \in N_p \qquad E_{PV}^{n,t} \leq C_{PV}^{n} \cdot \tilde{f}_{PV\text{-}EL}^{n,t} \tag{13}$$

$$\forall\, t, n \in N_p \qquad 0 \leq E_{grid}^{n,t} + E_{PV}^{n,t} \leq \frac{C_{PV}^{n} \cdot 24}{\tilde{r}_{PV\text{-}EL}} \tag{14}$$

$$\forall\, t, n \in N_p \qquad q_{prd}^{n,PV\text{-}EL,t} = \frac{E_{grid}^{n,t} + E_{PV}^{n,t}}{\widetilde{cons}_{EL}} \tag{15}$$

$$\forall\, t, n \in N_p \qquad E_{sur}^{n,t} = E_{PV,tot}^{n,t} - E_{PV}^{n,t} \tag{16}$$

The simultaneous presence of multiple transport modalities requires the definition of multiple mass balance equations (Eq. (18)). Indeed, a single production site may host different conditioning processes, connecting the node with the two transport networks, given that the sum of all conditioning flows must be equal to the production (Eq. (17)). The absence of an inlet flow to the storage ensures that production facilities are not exploited as pure storage nodes. To maintain a general approach, a loss term is considered for all storage options ($\tilde{\varepsilon}_s$), even though it is non-null only for liquid storage, which is affected by boil-off.

$$\forall\, t, p, n \in N_p \qquad q_{prd}^{n,p,t} = \sum_{m \in M} q_{cnd}^{n,m,t} \tag{17}$$

$$\forall\, t, m, n \in N_p \qquad Q_s^{n,t+1} = Q_s^{n,t} \cdot (1 - \tilde{\varepsilon}_s) + \left(q_{cnd}^{n,m,t} - q_{out,s}^{n,t}\right) \cdot \widetilde{\Delta t} \cdot \widetilde{N}_{td} \tag{18}$$

Eq. (18) shows how the typical day approach affects variables and mass balances. The evolution of the storage content in each node involves $|T| + 1$ items, in order to track both the beginning and the end of the simulated time frame. Accordingly, the variable $Q_s^{n,t}$ is a snapshot of the storage level before the daily flows of the first repetition of the typical day of time step $t$ occurs, thus representing the storage content at the beginning of the time step $t$, which is characterised by $\widetilde{N}_{td}$ repetitions of the associated typical day. Each repetition features identical flows and storage variations, but different storage content due to the cumulative effect. Given the assumption $|T| = 52$, the repetition of the typical day within the time step $t$ corresponds to a week of operation. Thus, $Q_s^{n,t+1}$ represents the snapshot of the storage level at the end of the week, which is also the beginning of the following one.

As Eq. (19) shows, the installed storage capacity at production nodes is bounded within a minimum and a maximum value that are related to the corresponding conditioning capacity. In this analysis, $\tilde{k}_{min,prd}^{s}$ and $\tilde{k}_{max,prd}^{s}$ are set to 1 and 4, respectively. A non-null lower boundary is adopted to ensure that, as it happens in practice, a certain capacity is always installed to compensate intraday mismatches between production and offtakes, which the time resolution of the model does not capture.

$$\forall\, m, n \in N_p \qquad \tilde{k}_{min,prd}^{s} \cdot C_{cnd}^{n,m} \cdot \tilde{f}_{conv}^{m} \leq C_s^{n} \leq \tilde{k}_{max,prd}^{s} \cdot C_{cnd}^{n,m} \cdot \tilde{f}_{conv}^{m} \tag{19}$$

Finally, the virtual sub-node balance determines the hydrogen flows distributed to the network edges:

$$\forall\, t, m, e, n \in N_p \qquad \tilde{Y}^{m,n} \cdot q_{edg}^{e,m,t} = q_{out,s}^{n,t} \tag{20}$$

### *4.2.2 Hydrogen storage*

Intermediate storage hubs require to track the stored content via mass balances. For the modalities $m = GP, LT$, these are expressed as:

$$\forall\, t, n \in N_s^m \qquad Q_s^{n,t+1} = Q_s^{n,t} \cdot (1 - \tilde{\varepsilon}_s) + \left(q_{in,s}^{n,t} - q_{out,s}^{n,t}\right) \cdot \widetilde{\Delta t} \cdot \widetilde{N}_{td} \tag{21}$$

$$\forall\, t, e, n \in N_s^m \qquad \tilde{Y}^{m,n} \cdot q_{edg}^{e,m,t} = q_{out,s}^{n,t} - q_{in,s}^{n,t} \tag{22}$$

As discussed in Section 3.2.2, intermediate storage is not envisaged for compressed hydrogen truck delivery, for which such nodes behave as pure transit points:

$$\forall\, t, e, n \in N_s^m \qquad \tilde{Y}^{GT,n} \cdot q_{edg}^{e,GT,t} = 0 \tag{23}$$

Excluding transit nodes, storage can be performed in all node types. In order to ensure the cyclic operation of the infrastructure, the stored hydrogen quantity at the end of the simulated time frame ($t_f$) must be equal to that at the beginning ($t_i$). The constraint is expressed as a not-smaller-than inequality (Eq. (24)), since a strict equality is numerically complex in presence of integer variables and it is also affected by the repetitions of typical days and the presence of storage losses. The consistency of results is anyhow preserved, since the excess of stored hydrogen would require additional production and is therefore avoided by the model.

$$\forall\, s, n \in N_p \cup N_s^m \cup N_d \qquad Q_s^{n,t_f} \geq Q_s^{n,t_i} \tag{24}$$

### *4.2.3 Demand points*

The binary variables $\xi^{n,m}$ ensure that each demand node receives hydrogen in one physical form only:

$$\forall\, n \in N_d \qquad \sum_{m \in M} \xi^{n,m} = 1 \tag{25}$$

These variables are used in the mass balance of demand nodes, which include a storage section with exclusively inlet flows and a virtual sub-node for connection to the graphs:

$$\forall\, t, m, n \in N_d \qquad Q_s^{n,t+1} = Q_s^{n,t} \cdot (1 - \tilde{\varepsilon}_s) + \left(q_{in,s}^{n,t} - \tilde{q}_{dem}^{n,t} \cdot \xi^{n,m}\right) \cdot \widetilde{\Delta t} \cdot \widetilde{N}_{td} \tag{26}$$

$$\forall\, t, m, e, n \in N_d \qquad \tilde{Y}^{m,n} \cdot q_{edg}^{e,m,t} = -q_{in,s}^{n,t} \tag{27}$$

As Eq. (28) shows, the storage capacity at demand nodes is bounded by a minimum and a maximum value, which are defined according to the transport modality. In particular, $\tilde{C}_{s,dem,min}^{n,m}$ is set to the capacity of a single truck for $m = GT, LT$, which corresponds to the minimum delivery, due to truck transport occurring with discrete values. For $m = GP$, such limit is set to zero. The upper boundary depends also on the case study application and is therefore discussed in Section 5.3. Consistently with Eq. (26), the binary variable $\xi^{n,m}$ ensures that storage is installed only for the exploited transport modality.

$$\forall\, m, n \in N_d \qquad \tilde{C}_{s,dem,min}^{n,m} \cdot \xi^{n,m} \leq C_s^n \leq \tilde{C}_{s,dem,max}^{n,m} \cdot \xi^{n,m} \tag{28}$$

Since the model time resolution does not track intraday flows, the storage at demand nodes is constrained to contain at least a fraction $\tilde{k}_{dem}^m$ of the daily demand (Eq. (29)). This allows to compensate the temporal mismatch between production and consumption, since the produced quantity $q_{prd}^{n,p,t}$ may not be entirely available at the beginning of the day, and, for road delivery, the time gap between transport and consumption, since trucks require additional time for parking, loading, and unloading, thus making the received quantity not immediately available. In this analysis, $\tilde{k}_{dem}^m$ is assumed equal to 1/3 for pipeline delivery and to 1/2 for road delivery, as the latter is affected by both mismatches.

$$\forall\, t, n \in N_d \qquad Q_s^{n,t} \cdot (1 - \tilde{\varepsilon}_s) \geq \tilde{k}_{dem}^m \cdot \tilde{q}_{dem}^{n,t} \cdot \xi^{n,m} \tag{29}$$

Note that, thanks to the typical day approach, it is sufficient to constrain with Eq. (29) just the stored quantity at the beginning of each week (i.e., $Q_s^{n,t}$), since, if the equation is satisfied in the first day of the week, it will also hold for the following ones (see Section 3.3.2).

#### *4.2.4 Hydrogen transport*

Transport pathways consist of a series of transit nodes connected through graph edges. Since these nodes do not provide any contribution to production, consumption, nor storage, the outgoing flow must equal the incoming one:

$$\forall\, t, m, e, n \in N_t^m \qquad \tilde{Y}^{m,n} \cdot q_{edg}^{e,m,t} = 0 \tag{30}$$

The number of trucks in motion per edge affects the operational costs for road delivery ($m = GT, LT$) in Eq. (9). Eqs. (31)-(32) compute the absolute values of the hydrogen flows along edges, which might assume negative values depending on the verse of the graph edges, while Eq. (33) calculates the number of trucks (integer) that must be employed to deliver the required hydrogen quantity. By avoiding integer variables to represent the hydrogen flows in road delivery (e.g., considering $q_{edg}^{e,m,t}$ for $m = LT, GT$ as integers), this approach reduces the model combinatorial complexity, with significant benefits on computational performances, since integer variables are excluded from the mass balances.

$$\forall\, e, t \qquad q_{edg}^{e,m,t} \leq q_{edg,ABS}^{e,m,t} \tag{31}$$

$$\forall\, e, t \qquad -q_{edg}^{e,m,t} \leq q_{edg,ABS}^{e,m,t} \tag{32}$$

$$\forall\, e, t \qquad N_{truck}^{e,m,t} \geq \frac{q_{edg,ABS}^{e,m,t}}{\tilde{C}_{truck}^{m}} \tag{33}$$

To determine the capital cost of the two road transport modalities, Eqs. (34)-(35) compute the (integer) number of cylinder- or tank-equipped trailers that must be purchased, respectively, which are then employed in Eq. (2) to compute costs. For compressed hydrogen truck delivery, storage is performed in the pressurized vessels of the transported trailers, which are filled at production sites and dropped off at demand points. Accordingly, the total number of required cylinder-equipped trailers coincides with the installed storage capacity for $s = GT$ (i.e., $C_{GT}^{n}$). The number of these trailers must account for both the stored ones and those that enter the network from production nodes, which are related to the operational quantities $q_{edg}^{e,GT,t}$ and $N_{truck}^{e,GT,t}$ through mass balances. The tank-equipped trailers of liquid hydrogen trucks are independent of the installed storage capacity, as they are emptied at delivery points in separated vessels. In this case, the number of trailers to be purchased is represented by the variable $C_{trailer,LT}^{n}$, which is the (integer) number of tank-equipped trailers that a production or storage node must own to deliver the required amount of liquid hydrogen.

$$\forall\, t, n \in N_p \cup N_d \qquad C_{GT}^{n} \geq \frac{Q_{GT}^{n,t+1} + q_{out,GT}^{n,t}}{\tilde{C}_{truck}^{GT}} \tag{34}$$

$$\forall\, t, n \in N_p \cup N_s^m \qquad C_{trailer,LT}^{n} \geq \frac{q_{out,L}^{n,t}}{\tilde{C}_{truck}^{LT}} \tag{35}$$

Finally, as pipelines deliver hydrogen at a lower pressure than that of storage vessels, a certain compression capacity must be installed at storage or demand nodes to process a quantity equal to the inlet storage flow:

$$\forall\, t, n \in N_s^m \cup N_d \qquad q_{cnd}^{n,GP,t} = q_{in,G}^{n,t} \tag{36}$$

# 5. Case study: assumptions and data

## 5.1. Scenario

The developed model is applied to a future scenario in which hydrogen is widely employed as a fuel for mobility, and a hydrogen infrastructure is required to supply a network of HRSs. The selection of such destination is driven by the growing attention to clean mobility [3], [31], [75], but the proposed model is not limited to this application, since the formulation is general and it can be adapted to investigate scenarios with different hydrogen end uses. Examples include industrial hydrogen demand in the steel and chemical sectors, integration with the power sector to supply hydrogen-based generation to compensate deficits or provide grid balancing services, use in aviation, etc.

The analysis investigates the regional case of Sicily in Italy, considering the long-term timeframe of year 2050 as reference for technological and economic parameters. The annual hydrogen demand is computed considering a projected presence of FCEVs corresponding to 30% of the passenger car stock in the country, with slight deviations among regions. The same overall hydrogen demand could also result from a different mix of passenger cars, heavy duty trucks, and local public transport. The distribution of the hydrogen consumption among provinces is estimated on the basis of factors such as population, income per capita, and vehicle ownership as detailed in Ref. [76]. The resulting regional demand in Sicily is 80 $kt_{H2}$ per year.

Figure 6 shows the directed graphs representative of the candidate HSC networks, which are built applying the methodology presented in Section 3.3.1, starting from the road network and the natural gas grid shapefiles of Sicily. The former is obtained from the Italian road network shapefile available in the DIVA-GIS database [77], while the latter is built through the vectorization of the European natural gas network [78], including pipelines belonging to both the regional and the national grid. As potential production nodes, the four refineries of Milazzo, Augusta, Priolo Gargallo, and Gela [79] are selected for SMR-CCS plants (purple diamonds in Figure 6), assuming that a fraction of their current hydrogen production capacity will be available as export for mobility, while the centroids of the nine provinces are considered as candidate locations for the installation of PV-EL systems (orange diamonds in Figure 6). As far as demand points are concerned, the position of existing gasoline/diesel refuelling stations is adopted as candidate location. According to a homogeneous spatial distribution, 10% of them are selected to host hydrogen refuelling, for a total of 80 HRSs in the region (blue-green dots in Figure 6). The hydrogen demand is distributed among provinces on the basis of population, population density, vehicle ownership rate, and income per capita [31] and then assigned homogeneously to the HRSs in each province. As a result, the demand of each HRS ranges between 0.5-1.9 $kt_{H2}$/y. The demand evolution throughout the year is tracked on the basis of monthly traffic data. Following the typical day approach (see Section 3.3.2), the daily demand is computed as the monthly average value and repeated identically for each day of the month. Finally, candidate storage nodes (yellow downward-pointing triangles in Figure 6) are selected among transit nodes through a random extraction, ensuring that they are evenly distributed, with a minimum distance from each other of 20 km.

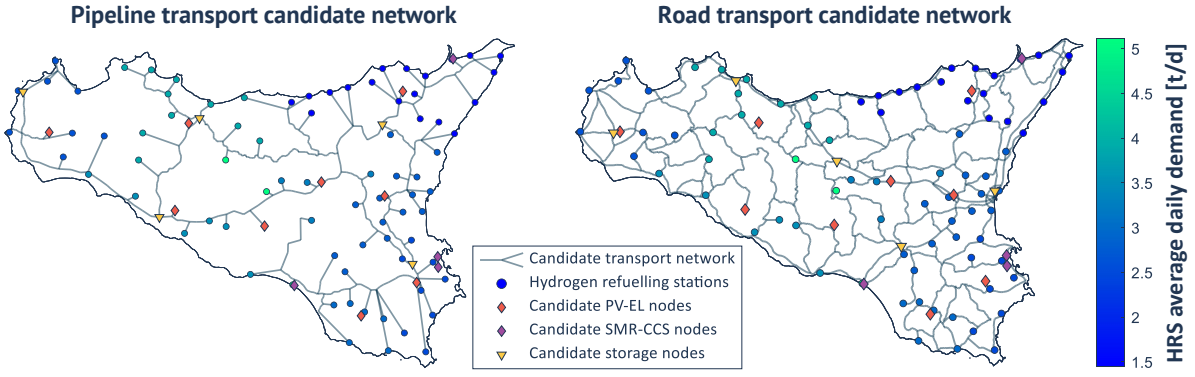


*Figure 6. Representative graphs of the candidate transport networks.*

### 5.2. Economic approach and policy framework

In order to compute the annuity of the capital costs, a capital recovery factor (CRF) is computed for each component of the HSC, considering the lifetime (variable for each component) and a discount rate of 8% (assumed fixed for all investments) [14]. On the contrary, operational costs are detailed according to the technical performance parameters and the actual operation.

The economic parameters employed in the model are collected from a variety of sources dating back to different years. To have a uniform set of data, all costs are converted into $€_{2019}$ by means of currency conversion rates and inflationary adjustments for either EU [80] or USA [81].

The model computes the $CO_2$ emissions associated with the production of blue hydrogen in SMR-CCS plants and with the generation of grid electricity, taking into account the application of a carbon tax within the OPEX. Grid electricity is employed in two separate instances: hydrogen conditioning and hydrogen production via electrolysis when PV generation is not available. These uses differ by the way in which power generation occurs, thus requiring the introduction of distinct emission factors. Considering that the RES share in the Italian electricity generation mix is expected to reach at least 80% by 2050 [82], the average $CO_2$ emission factor for electricity generation in 2050 is assumed to drop to 85.4 $g_{CO2}/kWh_e$ (from 284.5 $g_{CO2}/kWh_e$ in 2019 with a 33% RES share [83]). Such value, as an annual average, is deemed suitable to describe the generation that covers conditioning consumption that occurs variably throughout the day ($\tilde{e}_{E,cnd}$ in Eq. (10)), whereas electrolysers are likely to absorb grid electricity at night, when direct PV feeding is not available, thus suffering from a lower RES share due to the absence of solar input also within grid electricity generation. Hence, a 25% higher emission factor is assumed for this use, equal to 106.7 $g_{CO2}/kWh_e$ ($\tilde{e}_{E,EL}$ in Eq. (10)). The adopted emission factors and carbon tax are summarized in Table 2.

*Table 2. Input data: $CO_2$ emission factors and carbon tax.*

| Parameter | Range | Selected value | Unit | Ref. |
|---|---|---|---|---|
| SMR-CCS $CO_2$ emission factor | 1.0-4.3* | 1.0 | $kg_{CO2}/kg_{H2}$ | [14] |
| Electricity generation $CO_2$ emission factor (to CND) | - | 85.4 | $g_{CO2}/kWh_e$ | Own assumption |
| Electricity generation $CO_2$ emission factor (to EL) | - | 106.7 | $g_{CO2}/kWh_e$ | Own assumption |
| Carbon tax | 60-225 | 90 | €/ $t_{CO2}$ | [14], [84] |

*$CO_2$ capture rate ranging from 53.2% to 90% [12]

### 5.3. Techno-economic parameters

The technologies included in the HSC are characterised by different maturity levels. Although some components are still in the early stage of commercialization, the technological development and the increase in manufacturing volumes are expected to lead to an improvement of efficiencies and to a decrease of costs. Since the analysis looks at a long-term scenario, techno-economic data are selected exploiting available projections or adopting optimistic values among short-term estimates. The data are summarized and referenced in in this section, providing both the selected value and the proposed range of values to offer a broader context.

Techno-economic data for hydrogen production are reported in Table 3. Since green hydrogen is expected to cover the majority of the demand in long-term scenarios, with blue hydrogen playing a limited baseline role, it is assumed that refineries will offer 20% of their current hydrogen production capacity as available for export to mobility uses, implementing CCS. For PV-EL plants, the maximum PV capacity devoted to hydrogen production via electrolysis is assumed equal to five times the installed capacity in 2018 in each

province to ensure that the proportion among provinces is preserved, leading to a total of 7 $GW_e$. The installed electrolysis capacity is derived from that of the dedicated PV plant considering a fixed capacity ratio $\tilde{r}_{EL\text{-}PV} = 2$, which was optimized in a previous work [85] (see Appendix 1). The maximum installable capacity for each of the candidate production sites is shown in Figure 9.a. Table 3 also shows the adopted electricity purchase cost and sale price, which are assumed constant throughout the year for simplicity. A low sale price is considered to account for the fact that this surplus generation will need to compete in a highly dynamic market in the projected long term of very large RES installation, where the PV generation peaks will be aligned for all plants.

*Table 3. Input data: hydrogen production.*

| Parameter | Range | Selected value | Unit | Ref. |
|---|---|---|---|---|
| SMR-CCS production cost | 1.6-1.9 | 1.9 | €/$kg_{H2}$ | [12] |
| SMR-CCS lifetime | 25 | 25 | y | [19] |
| Electrolysis CAPEX | 380-600 | 580* | €/$kW_e$ | [16] |
| Electrolysis fixed OPEX | 1%-5% | 2% | of CAPEX/year | [16] |
| Electrolysis specific consumption | 45-50.5 | 49 | $kWh_e/kg_{H2}$ | [16] |
| Electrolysis lifetime | 10-20 | 20* | y | [86] |
| PV CAPEX | 150-430 | 300 | €/$kW_e$ | [87] |
| PV fixed OPEX | 13 | 13 | €/$kW_e$/y | [88] |
| PV lifetime | 25-30 | 25 | y | [89] |
| Electricity purchase cost | 120-250 | 150 | €/$MWh_e$ | [90], [91] |
| Electricity sale price | 0-160 (year 2020) | 20 | €/$MWh_e$ | [90] |

*Includes stack replacement after 10 years

As discussed in Section 4.1, the economies of scale of liquefaction plants are represented with a single-trait linearization, considering a restricted capacity range. In particular, the range 10-100 $t_{H2}$/d is considered in the analysis, as preliminary simulations showed installed production capacities of this order of magnitude. Table 4 reports the values for the coefficients employed in Eq. (3) to linearize the liquefaction cost function with a scale factor of 0.615, which is an average of the values typically found in the literature [29], [30]. The resulting linearization is depicted in Figure 7, from which it emerges that the introduced error is minimal. As opposed to liquefaction, compression features a very high scale factor (0.9 [30]) and its CAPEX can be linearized for any capacity introducing only a small error. For the electricity consumption of compression, which drives the operational expenditures, an average compression efficiency of 63% is considered to account for the combined effect of typical commercial values of adiabatic, volumetric, electric, and organic efficiency.

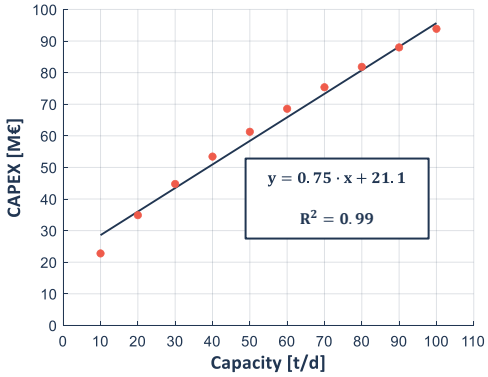


*Figure 7. Liquefaction CAPEX linearization.*

*Table 4. Input data: hydrogen conditioning.*

| Parameter | Range | Selected value | Unit | Ref. |
|---|---|---|---|---|
| Compression CAPEX | - | 1457.5 | €/$kW_e$ | [30] |
| Compression fixed OPEX | 4% | 4% | of CAPEX/year | [30] |
| Compression efficiency | - | 63% | - | Average commercial value |
| Compression lifetime | 15 | 15 | y | [45] |
| Liquefaction CAPEX | | | See Eq. (3) | |
| Liquefaction scale factor | 0.57-0.66 | 0.615 | - | Average literature value |
| $\widehat{capex}_{var,LIQ}$ | - | 0.75 | M€/(t/d) | From linearization |
| $\widehat{capex}_{fix,LIQ}$ | - | 21.1 | M€ | From linearization |
| Liquefaction fixed OPEX | 4% | 4% | of CAPEX/year | [30] |
| Liquefaction consumption | 6-11 | 6 | $kWh_e/kg_{H2}$ | [20] |

The assumed data for hydrogen transport are reported in Table 5. In the case of pipeline delivery, the dependence on the pipeline section is linear and can thus be directly employed in the MILP formulation. As far as pressure levels are concerned, existing natural gas pipelines are operated up to 75 bar in Italy; for hydrogen, pressure is assumed in the order of 100 bar at the inlet and 70 bar at the outlet [29], without detailing the pressure losses as a function of the flow rate since that would require a different level of analysis. Thus, intermediate recompression facilities are neglected, also thanks to the fact that distributed production allows to have multiple entry points where pressure is controlled (the Italian natural gas grid is equipped with recompression stations every 250 km, but most of them are rarely used and the main operation regards those at international import points). For both road transport modalities, a kilometric cost of 1.6 €/km is considered to account for fuel consumption, driver's salary, and rental cost of the tractor, assuming an average driving speed of 50 km/h. The CAPEX for compressed hydrogen trucks and liquid hydrogen trucks reported in Table 5 refer to the purchase of cylinder- and tank-equipped trailers.

*Table 5. Input data: hydrogen transport.*

| Parameter | Range | Selected value | Unit | Ref. |
|---|---|---|---|---|
| $H_2$ pipelines CAPEX | | See Eq. (4) | | |
| $\widetilde{capex}_{var,GP}$ | - | 4000 | k€/m²/km | From [30] |
| $\widetilde{capex}_{fix,GP}$ | - | 336 | k€/ km | From [30] |
| $H_2$ pipelines fixed OPEX | 4%-5% | 4% | of CAPEX/year | [29] |
| $H_2$ pipelines lifetime | 40-50 | 40 | y | [14] |
| Compressed $H_2$ trailers CAPEX | 355-600 | 400 | €/$kg_{H2}$ | Average literature value |
| Compressed $H_2$ trucks fixed OPEX | 2% | 2% | of CAPEX/year | [29] |
| Compressed $H_2$ trucks pressure | 250-540 | 500 | bar | [20] |
| Compressed $H_2$ trucks capacity | 300-1000 | 1000 | $kg_{H2}$/truck | [22] |
| Compressed $H_2$ trucks lifetime | 12-30 | 30 | y | [20] |
| Liquid $H_2$ trailers CAPEX | 200-260 | 207 | €/$kg_{H2}$ | [29] |
| Liquid $H_2$ trucks fixed OPEX | 2% | 2% | of CAPEX/year | [29] |
| Liquid $H_2$ trucks capacity | 4000-5250 | 4300 | $kg_{H2}$/truck | [29] |
| Liquid $H_2$ trucks lifetime | 12-30 | 30 | y | [20] |
| Truck rental cost | - | 1.6 | €/km | Average commercial value |

When destined to or coming from pipeline delivery, hydrogen is stored in Type 1 vessels at 160 bar, while in the case of transport via compressed hydrogen trucks, the cylinder-equipped trailers are exploited also as storage facilities (see Section 3.2.2). Liquid hydrogen is stored in cryogenic insulated tanks, which are filled from the trucks used for the delivery. Energy consumption related to compression via pumping is assumed to be negligible, whereas these systems are affected by a non-negligible daily boil-off loss equal to 0.1% of the stored quantity [14]. All assumptions related to hydrogen storage are reported in Table 6.

*Table 6. Input data: hydrogen storage.*

| Parameter | Range | Selected value | Unit | Ref. |
|---|---|---|---|---|
| Compressed $H_2$ storage CAPEX | 355-405 | 355 | €/$kg_{H2}$ | [22] |
| Compressed $H_2$ storage fixed OPEX | 2% | 2% | of CAPEX/year | [29] |
| Compressed $H_2$ storage pressure | 135-500 | 160 | bar | [20] |
| Compressed $H_2$ storage lifetime | 20-30 | 30 | y | [20] |
| Liquid $H_2$ storage CAPEX | 15-50 | 26 | €/$kg_{H2}$ | [29] |
| Liquid $H_2$ storage fixed OPEX | 2% | 2% | of CAPEX/year | [14] |
| Liquid $H_2$ storage boil-off | 0.03-0.10% | 0.10% | of stored $H_2$/d | [14] |
| Liquid $H_2$ storage lifetime | 20 | 20 | y | [29] |

The present analysis assumes that the delivered hydrogen is used for clean mobility, feeding FCEVs at hydrogen refuelling stations, which are therefore the final stage of the supply chain. As previously discussed, the detailed HRS management in terms of frequency of FCEV access and internal operation of the pressure-cascade tanks [92] are outside the boundary of the model, thus allowing to adapt the proposed formulation to investigate also the development of a HSC supporting different end uses. To include a realistic representation of the HRSs, the upper boundary of their installed storage capacity ($\tilde{C}^{n,m}_{s,dem,max}$ in Eq. (28)) is properly set according to the transport modality. For pipeline transport, the limit is the maximum daily

demand throughout the year in each node. For liquid hydrogen transport, the limit is the highest value between the maximum daily demand throughout the year in that node and the capacity of a truck, because the latter is the smallest possible daily delivery, as discussed in Section 4.2.3. Since liquid hydrogen trucks feature a large capacity, such a limit is sufficient to ensure that, considering the daily demand of the analysed case study, a single HRS does not receive more than two trucks per day. The upper boundary for gaseous truck delivery is set equal to the capacity of 3 trucks in order to take into account a reasonable constraint on land occupation, considering that such delivery modality consists of dropping off the cylinder-equipped trailers at the station. Altogether, these assumptions prevent the creation of large hubs at demand nodes. At the same time, the presence of candidate intermediate storage nodes guarantees the possibility of having a flexibility element in the HSC and possibly of creating hydrogen hubs, which may become even more important when different types of demand points are combined.

As far as costs are concerned, demand nodes are characterized only by the expenditures related to storage and compression, as it is assumed that the installation cost for the different types of stations is not significantly different.

## 6. Results and discussion

The proposed model is employed to investigate the infrastructural needs arising from a 30% stock share of FCEVs among passenger cars in the Italian region of Sicily. The optimization problem is solved in 63 computational hours exploiting a workstation equipped with an Intel Core i9-10980XE processor and 64 GB RAM.

### 6.1. Hydrogen infrastructure design and operation

The optimal infrastructure configuration relies on the parallel use of all the included transport modalities. As Figure 8 shows, 50 of the 80 HRSs are supplied via pipeline, 17 via compressed hydrogen truck, and the remaining 13 via liquid hydrogen truck. Despite supplying 21% of the stations, compressed hydrogen delivered via truck accounts for only 11% of the total hydrogen demand, since this modality is exploited for small stations due to both the high specific cost, which makes it suitable for relatively low delivery requirements, and the upper boundary on the storage capacity discussed in Section 5.3. On the contrary, pipeline delivery is employed for large stations, as it represents 72% of the total demand while supplying 63% of the stations, whereas the consumption share of liquid hydrogen reflects the percentage of supplied stations.

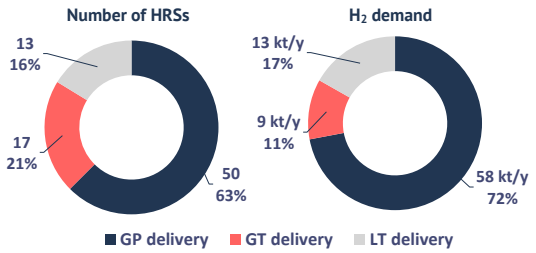


*Figure 8. Number of HRSs and fraction of hydrogen demand supplied by transport modality.*

Table 7 summarizes the design parameters of the infrastructure and the related investments, while Table 8 provides the main results concerning the operation of the supply chain. As expected, the capacity of the SMR-CCS plants is saturated thanks to the low production cost, and they operate at base-load capacity throughout the year. Given the assumed boundaries on refineries' export capacity, the overall SMR-CCS production is limited to 21 $kt_{H2}/y$, covering 26% of the regional hydrogen demand. Accordingly, most of the production is provided by electrolysis systems. The installed capacity of dedicated PV is 2.2 $GW_e$, corresponding to

approximately 30% of the assumed upper boundary, as it emerges also from Figure 9, which shows that none of the installed PV-EL plants saturates the available potential. The capital expenditures of PV plants and electrolysis systems are comparable, due to the different specific investment cost. Combined, PV-EL systems account for more than half of the overall investment required for the development of the infrastructure. Electrolysers mainly rely on electricity generated from PV, while the import from the grid is below 1% of the overall consumption due to the high purchase price that results from both the grid price and the carbon tax. The installed PV capacity guarantees a generation surplus of 651 $GWh_e$/y, which leads to revenues for 13 M€/y, corresponding to 11% of the overall annual operational expenditure.

*Table 7. Optimal infrastructure configuration: capacities and investment costs by component.*

| Design parameter | Capacity | Investment cost [M€] |
|---|---|---|
| PV | 2.2 $GW_e$ | 656 |
| Electrolysis | 1.1 $GW_e$ | 634 |
| SMR-CCS | 71 $t_{H2}$/d | 113 |
| $GPH_2$ compression | 23 $MW_e$ | 33 |
| $GTH_2$ compression | 3 $MW_e$ | 5 |
| Liquefaction | 43 $t_{H2}$/d | 74 |
| $GPH_2$ storage | 272 $t_{H2}$ | 97 |
| $GTH_2$ storage | 70 $t_{H2}$ | included in '$GTH_2$ trailers' |
| $LH_2$ storage | 545 $t_{H2}$ | 14 |
| Pipeline network | 1166 km | 430 |
| $GTH_2$ trailers | 70 | 28 |
| $LTH_2$ trailers | 15 | 13 |
| Total | - | 2097 |

*Table 8. Optimal infrastructure configuration: main operational parameters.*

| Parameter | Value |
|---|---|
| SMR production | 21 $kt_{H2}$/y |
| PV-EL production | 59 $kt_{H2}$/y |
| Grid electricity to PV-EL systems | 10 $GWh_e$ |
| Total PV electricity | 3537 $GWh_e$ |
| PV electricity consumed by electrolysis | 2887 $GWh_e$ |
| PV electricity surplus | 651 $GWh_e$ |
| Highest number of $GH_2$ trucks in motion per day | 33 |
| Highest number of $LH_2$ trucks in motion per day | 16 |

Figure 9 compares the distribution and the nominal capacities of the installed hydrogen production plants (Figure 9.b) with the available potential in the region (Figure 9.a) that results from the assumptions discussed in Section 5.1. While the entire SMR-CCS capacity is saturated, electrolysis plants are installed in seven of the nine available sites, as Enna (EN) and Caltanissetta (CL) are not exploited. This shows that, in the production of green hydrogen, the optimal configuration seeks an equilibrium between a widespread positioning that shortens delivery distances and an increase in plant sizes that decreases storage and equipment needs. By comparing the nominal capacities with the HRSs demand requirements reported in Figure 6, it emerges that the largest plants are installed where the stations with the highest demand are

located, i.e., in the proximity of Palermo (PA), and in areas characterized by a high concentration of HRSs, such as the central-eastern part of the region, i.e., Catania (CT) and Siracusa (SR).

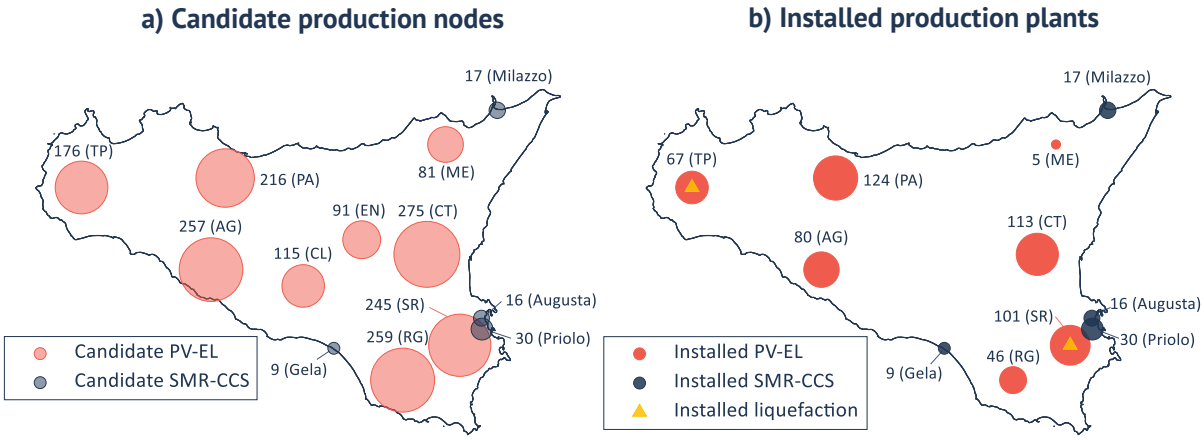


*Figure 9. Locations and capacities (in $t_{H2}$/d) of the hydrogen production plants: (a) available potential, (b) installed capacity in the optimal configuration.*

Figure 10 shows the optimal transport networks for each of the exploited transport modalities, highlighting the demand, production, and intermediate storage nodes that are connected to each network (labelled "active" in the figure). With an overall extension of more than 1100 km, the installed pipeline network (Figure 10.a) spans the entire region and is connected to all the production facilities. Pipelines supply the stations with the highest demand requirements (green dots in Figure 10), as their installation is economically justified only for large demand hubs due to the high capital cost. Two shorter pipelines are also realized to supply two HRSs in the north-eastern part of the region, exploiting two of the smallest production plants, i.e., the PV-EL system of the province of Messina (ME in Figure 9) and the Milazzo refinery. The size of the installed pipelines is reported in Figure 10.b. The largest tracts have a diameter of about 20 cm and are connected to the main production nodes, from which hydrogen is transported to HRSs with progressively smaller tubes, reaching a minimum diameter of 6 cm.

Truck delivery benefits from a wider range of candidate routes thanks to the greater extension of the road network. Accordingly, the exploited pathways for both compressed and liquid hydrogen trucks are more branched than the installed pipeline network. As Figure 10.c shows, compressed hydrogen trucks are employed to supply a limited network of HRSs in the north-eastern part of the region. Such stations are characterized by a low demand, confirming that this transport modality is suitable to meet relatively small delivery requirements over short-medium distances. On the contrary, liquid hydrogen trucks are exploited to deliver hydrogen across the entire region (Figure 10.d), as they are competitive for long-distance transport thanks to the larger capacity. As Figure 9 shows, liquefaction is installed in only two of the eleven production sites, as its capital-intensity and economies of scale push the optimization towards larger installations. Liquefaction represents the highest conditioning expenditure, even if liquid hydrogen accounts for a smaller consumption share than pipeline delivery (see Figure 8 and Table 7). Nevertheless, the high investment is compensated by the low storage cost, which results in an installed storage capacity of 545 $t_{H2}$, which is considerably higher than that for both GP and GT delivery. In particular, more than 360 $t_{H2}$ are installed at four intermediate sites, and, as Figure 10 shows, liquid hydrogen is the only modality for which such option is exploited. The four intermediate sites have a capacity of 27, 44, 120, and 172 $t_{H2}$, and they are exploited to absorb the overproduction of PV-EL plants in the central part of the year. Comments on seasonality effects and storage use are provided in Appendix 3.

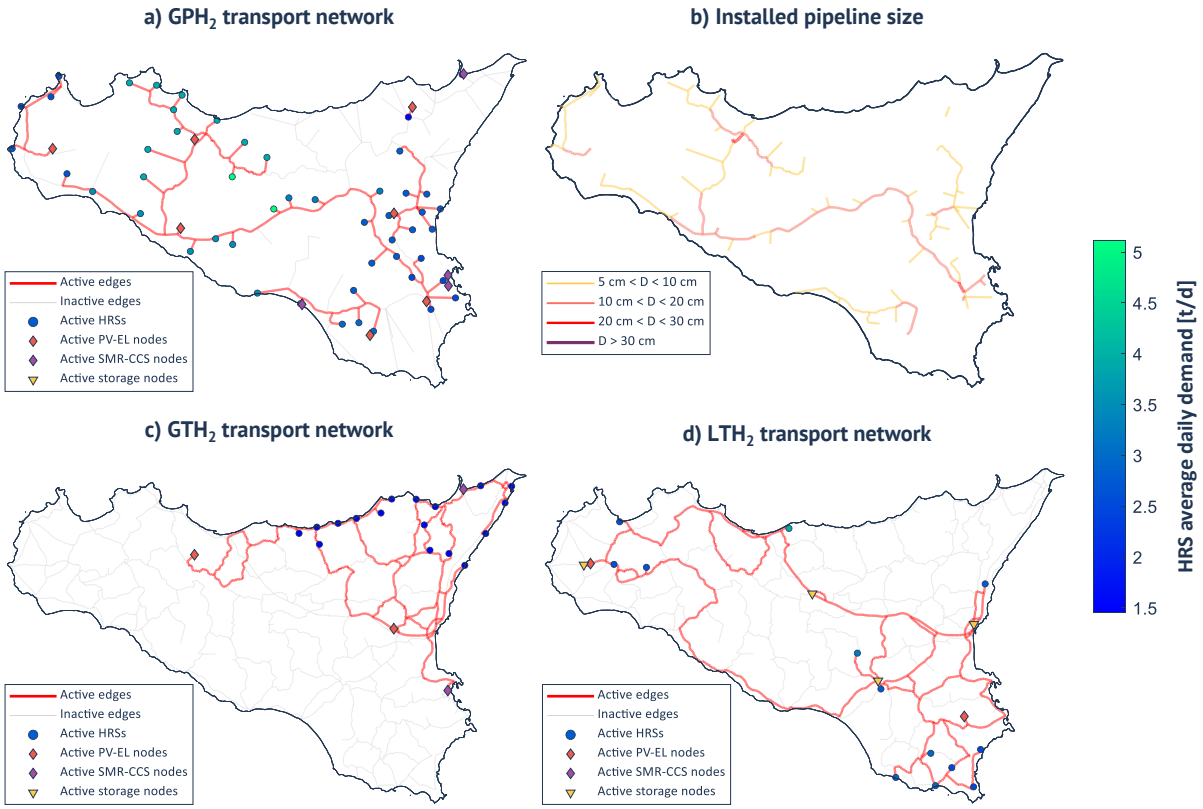


*Figure 10. Optimal transport networks (a, c, d) and size of the installed pipelines (b).*

The impact of the HSC operation on the road infrastructure can be represented by the number of trucks in motion per day. As reported Table 8, in the highest amounts throughout the year for GT and LT delivery are 33 and 16 trucks, respectively. Since such values are reached in different days (see Figure 11), the peak traffic in the network corresponds to 48 trucks. As an average, the number of trucks in motion per day is 39, thus impacting marginally on the road infrastructure of the region. Furthermore, Figure 11 shows that the traffic is higher during summer, i.e., when the mobility sector has its demand peak. Considering the operation of hydrogen refuelling stations, the receiving bays are not overloaded, since the peak values are reached few times throughout the year, and the average number of trucks per day per station is below 1 and 2 for LT and GT delivery, respectively.

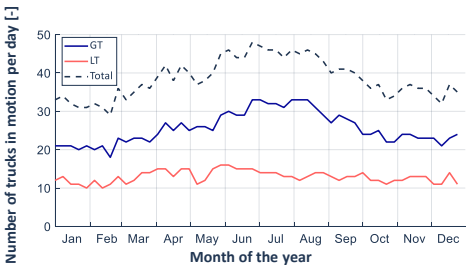


*Figure 11. Number of trucks in motion per day.*

## 6.2. Cost of hydrogen

The optimal infrastructure configuration combines the three transport modalities and yields an average cost of hydrogen delivered to HRSs of 3.81 €/$kg_{H2}$. This comprises all capital and operational expenditures related to production, transport, and storage, as described in Section 4.1. Figure 12 details the breakdown of the

average cost of hydrogen. In particular, the three bars on the left show the cost breakdown for the HRSs supplied via GP, GT, and LT delivery, respectively, while the bar on the right is the average for the entire HSC, i.e., considering all demand points. Costs in the figure comprise both CAPEX and OPEX of each stage of the supply chain, while the percentage values are the cost share of each item in the corresponding bar. Note that the mean of the average costs by transport modality (three bars on the left in Figure 12) weighted on the respective share on the total hydrogen demand (right doughnut chart in Figure 8) yields the average specific cost for the entire HSC (bar on the right in Figure 12).

The most relevant cost item is production, which amounts to 2.40 €/kg$_{H2}$. Considering the cost breakdown of the entire HSC, this corresponds to 64% of the total. In particular, the greatest contribution to the production expenditure is the installation of dedicated PV capacity, which alone weighs approximately 0.80 €/kg$_{H2}$, about 20% of the total, whereas electrolysis investments account for an additional 0.80 €/kg$_{H2}$. Thus, the contribution of integrated PV-EL system CAPEX exceeds 40% of the overall cost. These results are consistent with the investment agenda of the European Commission, according to which the production of green hydrogen through P2H facilities will be the highest-share expenditure in the development of a hydrogen economy [7].

Overall, conditioning covers 14% of the final cost, mainly due to investment and consumption of liquefaction, which represents more than 50% of the conditioning expenditure in the entire HSC. Indeed, conditioning is the highest-share item for HRSs supplied via LT delivery (third bar in Figure 12), corresponding to 1.57 €/kg$_{H2}$ for the distributed liquid hydrogen, whereas for GP and GT delivery it amounts to less than 0.50 €/kg$_{H2}$.

Hydrogen transport is the second largest cost item, accounting for 0.70 €/kg$_{H2}$ overall (17%). Such component is particularly relevant for GP delivery (0.77 €/kg$_{H2}$, first bar in Figure 12), mainly due to installation CAPEX. The transport share is significant also for GT delivery (0.66 €/kgH2, second bar in Figure 12), which, however, does not require additional storage expenditures, since storage is performed in the same cylinder-equipped trailers exploited for transport. Thanks to the higher energy density, transport costs for liquid hydrogen delivery are limited to 0.19 €/kg$_{H2}$. For both road delivery options, the transport expenditure is evenly divided between CAPEX, i.e., the purchase of cylinder- or tank-equipped trailers, and OPEX, i.e., expenses related to fuel consumption, driver's salary, tractor renting, and O&M.

The storage cost (0.15 €/kg$_{H2}$) accounts for the installed capacity at production sites, intermediate hubs, and refuelling stations. This is absent for compressed hydrogen truck delivery since trailers are already accounted for in the transport item. The expenditure in the cases of GP and LT delivery is comparable since, although specific storage costs are lower for liquid hydrogen, the discrete nature of this transport option requires a larger storage capacity at demand nodes (i.e., at least the capacity of a single liquid hydrogen truck, assuming that partial emptying is not envisaged).

Finally, the carbon tax component is the least relevant, weighing about 1% of the total cost, since the infrastructure mainly relies on green hydrogen, and electricity consumption for conditioning is a minor term.

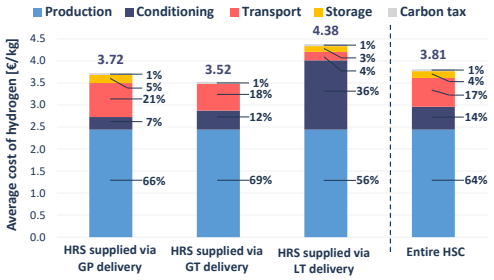


*Figure 12. Breakdown of the average cost of hydrogen delivered to HRSs, considering the HRSs supplied by each transport modality and the overall HSC.*

The model allows selecting which transport modalities to include in the optimization. As discussed, the optimization with all three options active employs all of them in the supply chain. Comparing the results for

such multi-modality infrastructure with those from simulations of mono-modality supply chains allows to assess the advantage of a more complex combination. In particular, the exclusive presence of pipelines yields an average cost of hydrogen equal to 4.00 €/$kg_{H2}$ (+5%), whereas a system exploiting only liquid hydrogen features a value of 4.16 €/$kg_{H2}$ (+9%). A supply chain that relies only on transport via compressed hydrogen trucks is, instead, unfeasible under the storage and delivered trucks constraints.

### 6.3. Total infrastructure costs

As reported in Table 7, the overall investment required for the infrastructure realization is approximately 2.1 G€. PV installation is the largest expenditure item, accounting for more than 30% of the investment. However, this expense should not be entirely allocated to the hydrogen infrastructure due to the significant interaction that the installed PV capacity has with the electric grid, as the resulting surplus electricity corresponds to approximately 18% of the total generation from the additional PV installation and 4% of the region's annual electricity consumption [93]. From a broad perspective, these results suggest that sector coupling might be extremely valuable to support the massive penetration of renewable sources in the energy system.

The observed investment appears in line with the expenditures that are typically related to infrastructural interventions: for example, *Terna SpA*, the Italian electric grid TSO, has planned to invest 8.9 G€ between 2021 and 2025 for infrastructural upgrades across Italy [94], while 7.4 G€ are foreseen between 2020 and 2024 by *Snam SpA* for the evolution of the Italian natural gas grid [95]. The magnitude of the investment can be assessed by comparing its value with the gross domestic product (GDP) of the region, which was 88-89 G€ between 2017 and 2019. In this perspective, the investment does not appear unbearable, since it would represent approximately 2.4% of the GDP, and the annual impact would be limited to 0.1%, assuming that the expenditure will be spread over 20 years and that the GPD will not vary significantly. Furthermore, a more precise assessment should consider also the positive influence that the infrastructure realization and operation would bring to the economy in terms of value added and job creation [96].

### 6.4. Role of intermediate hydrogen storage

As Figure 10 shows, the optimal HSC configuration in the analysed case study exploits intermediate storage only in the form of liquid hydrogen, which features a considerably lower investment cost if compared to gaseous hydrogen (see Table 6). Indeed, results show that the capital cost of pressurized vessels is too high to favour the creation of intermediate hubs in the optimization, as the oversizing of PV-EL systems and their operation with the purchase of grid electricity is more beneficial to compensate the intermittency of solar radiation.

However, other economically competitive storage options will emerge in the future, thanks to cost reduction of existing technologies and development of new solutions to commercial maturity [14]. For example, capital cost estimates for underground hydrogen storage in lined rock caverns (LRCs) are in the order of 40 €/$kg_{H2}$ [23], corresponding to nearly 10% of the cost of pressurized vessels. To assess the impact of such a cost reduction, a mono-modality simulation imposing pipelines as the exclusive delivery option is performed, adopting the mentioned LRC projection as specific investment cost for gaseous hydrogen storage, while keeping all other input data unvaried. Results show that the availability of storage with low specific CAPEX leads to the exploitation of four out of five candidate intermediate sites, while a slightly smaller capacity of PV-EL systems is installed and their use of grid electricity is minimized. In other words, the intermediate storage facilities absorb the fluctuations of PV-EL hydrogen production, improving the operation of such systems.

Although this application should be complemented with a proper assessment on the suitable areas for LRC construction, it shows that storage hubs have a positive effect on the overall configuration and the current constraints mostly come from the economics, since intermediate storage is exploited when the cost is

competitive with that of hydrogen production. It should also be considered that, in the case study, seasonal storage needs are modest because the demand variation is positively correlated to the solar resource availability (higher in summer months), as discussed in Appendix 3. Going beyond the analysed case, the role of storage hubs could become pivotal in scenarios with stable demand profiles, as, for example, when industrial demand is considered.

## 7. Conclusions

This work presented a spatially and temporally resolved techno-economic optimization model of the hydrogen supply chain, which considers all stages from production to demand and includes multiple technological alternatives for production, transport, and storage. The primary objective of the study was the development of a multi-modality formulation that takes into account the parallel use of different technologies to minimize the cost of the infrastructure. This formulation is combined with the georeferenced modelling of the supply chain components and with the time-dependent analysis of the infrastructure operation over a year-long time frame with daily resolution. The simultaneous consideration of all these modelling features is a critical novelty aspect with respect to the existing literature on HSC. This could provide policy makers with a powerful tool to support the development of a cost-optimal hydrogen infrastructure, taking into account accurate cost estimates for both design and operation.

As a case study, the model was applied to investigate the infrastructural needs arising from hydrogen-based clean mobility in the Italian region of Sicily, considering a long-term (2050) scenario with a demand equivalent to a 30% stock share of FCEVs among passenger vehicles. Consistently with the European strategies, hydrogen production is provided for the largest part by electrolysis systems integrated with PV plants. The production of blue hydrogen via SMR equipped with CCS is also included, assuming that 20% of today's hydrogen production at existing refineries will be available for export. Results showed that the optimal infrastructure configuration simultaneously exploits all transport technologies, with 63% of HRSs supplied via pipeline, 21% via compressed hydrogen truck, and 16% via liquid hydrogen truck. Hydrogen production via PV-EL systems covers 74% of the consumption, while the available capacity of SMR-CCS is saturated to provide baseline production. The resulting average cost of hydrogen delivered to demand points is 3.81 €/$kg_{H2,}$ which in line with international targets (e.g., the US Department of Energy suggests a combined cost of production and delivery below 4 \$/$kg_{H2}$ to be economically competitive with other fuels for light-duty vehicles [20]). The economics of the infrastructure can further improve when taking into account sector coupling between power generation, transport, buildings, and industry.

The model application proves that the multiplicity of transport and storage technologies is a valuable asset in the development of a hydrogen economy, implying that they should be considered complementary rather than competing, as each may have different favourable applications, and their integration allows to reduce the average cost of delivered hydrogen. This is exemplified by the case study, which showed that the advantages of each technology are exploited in the optimal HSC configuration: pipelines deliver large quantities over long distances, liquid hydrogen is stored in large amounts at low cost, and compressed hydrogen trucks supply restricted networks of stations characterized by low demand.

Thanks to the general and flexible model formulation, this work lays the groundwork for multiple future analyses. The developed methodology can be applied to broaden the spectrum of available technological alternatives, since LOHC transport, biomass-based production, and wind-based electrolysis could be introduced following the modelling approach adopted for liquid hydrogen transport, SMR-CCS production, and PV-EL systems, respectively. Moreover, thanks to the adopted schematization of demand nodes, the model could be applied to diverse scenarios, characterized by different demand requirements and profiles. In this sense, the natural evolution of this work is to consider the infrastructural needs arising from the adoption of hydrogen in other sectors, such as power generation, building, and industry, aiming to determine to what extent sector integration could reduce the cost impact of the hydrogen infrastructure and foster its development. In addition, the geographical span can be enlarged to assess a country-wide optimal scenario.

## Appendix 1: PV-EL integration

Among the hydrogen production methods, this work investigates the adoption of electrolysis systems (EL) fed by clean electricity from solar photovoltaic plants (PV). This combination enables the development of large yet distributed hydrogen production systems, thanks to the modularity of both devices and the spread availability of the solar resource.

The integrated system is strongly dependent on the intra-day variations of electricity generation. Indeed, the PV power output features a daily bell-shaped profile, with height and width that vary throughout the year. In particular, the peaks differ according to the seasonal changes in irradiance, whereas the width follows the daytime hours. Both effects depend on latitude and location. Weather also affects electricity generation, possibly introducing steep and irregular variations. Figure A.1 shows two examples of PV generation profiles in two days characterized by high and low irradiance, respectively.

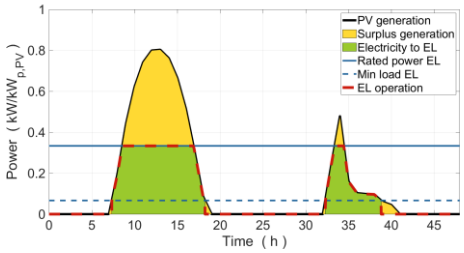


*Figure A.1. Example of integration between PV electricity generation and EL operation. The y-axis represents relative values with respect to the PV rated capacity.*

The amount of electricity that can be exploited by the electrolyser to generate hydrogen depends upon the nominal capacities (rated power) of both the EL unit and the PV field, so the design of integrated PV-EL systems can be parameterized on their ratio.

The interaction between the two plants is represented in Figure A.1, assuming a PV/EL nominal capacity ratio equal to 3. When the PV output is between the EL minimum load and the EL nominal capacity, the entire electricity generation feeds the electrolyser (green area), whereas in hours of very low or very large generation there is excess electricity (yellow area). Such surplus can be sold or curtailed. If hydrogen production is not required to originate entirely from local PV, the electrolyser can also purchase electricity from the grid at appropriate times (e.g., inexpensive market price), as long as its capacity is not already saturated by PV. This can increase the EL capacity factor, favouring the economics.

The cost of the produced hydrogen depends on both the installed capacities and the operation (O&M, compression consumption, surplus sale, etc.). Given the interaction constraints, the system components can be sized via cost optimization. Hydrogen storage must be taken into account since a highly variable operation is expected and it is unlikely that the supply chain can always absorb the instantaneous production. Results vary whether exclusive PV supply is imposed or grid electricity can be used. Moreover, revenues from surplus electricity have a significant role, although it is difficult to predict the sale price (excess generation would occur in central hours of the day, simultaneously with many other solar plants [97]).

Results from previous studies [15] on a mid-latitude location (such as Italy, 40-45°N) showed that, when the integrated system aims at a 100% RES-based hydrogen production with a low or null revenue from surplus electricity sale, the optimal design in terms of final LCOH is obtained at PV/EL nominal capacity ratio close to 2. Even when the use of grid electricity is allowed, the exploitation of local PV generation is always beneficial for hydrogen production, with an optimal share above 70-80%. When the electricity sale prices are high, the system design achieves low LCOH adopting a very large PV/EL nominal capacity ratio; however, this corresponds to a system that obtains most revenues from the electricity market. At low electricity sale prices, the optimal design favours smaller PV capacities, reducing the investment costs.

Based on the previous considerations, a procedure is here developed to properly describe the integrated PV-EL systems in the HSC model. The main aspect to deal with is the time resolution, since the model adopts a daily description, whereas PV-EL plants cannot neglect the hourly variability.

Production nodes that rely on PV-EL systems are defined by means of the installed capacities of the two plants, of which only the PV rated power is a decision variable, since a fixed PV/EL ratio of 2 is assumed to limit the configuration options and avoid non-linear relations. Possible effects of different values of this ratio could be further investigated in future works. To produce hydrogen, PV-EL production nodes primarily exploit electricity from the PV field, whose generation differs depending upon the location and the time of the year. Afterwards, the electrolysis system could saturate its capacity by purchasing grid electricity, taking into account the indirect $CO_2$ emissions related to the average electricity generation in the country or region. To assess the use of PV generation up to the saturation of the EL capacity, hourly or finer data are necessary, since PV peaks above the EL nominal power cannot be absorbed. However, the infrastructure model does not implement an intra-day focus. Hence, appropriate input data must be provided.

The input data for the infrastructure model are the time series of the daily electricity generation from PV ($\tilde{f}^{n,t}_{PV,tot}$) and the maximum amount of PV electricity that can feed the electrolyser ($\tilde{f}^{n,t}_{PV\text{-}EL}$) in each node $n$ and at each time step $t$, both expressed in relative terms on the installed PV capacity ($kWh_e/d/kW_{p,PV}$). The second value must, by definition, be equal to or smaller than the first. Based on the year-long hourly profiles described above, daily profiles are generated by summing the hourly data over each 24-hour period corresponding to one day. This allows to take into account the capacity limits and avoids the spreading of PV generation over the day to feed the electrolyser, which would require electric energy storage systems, with the related investment cost. Finally, the average weekly values are computed to obtain the 52 typical days employed in the HSC optimization model. These data depend on the PV location, so different profiles must be provided for each candidate PV-EL hydrogen production node.

Thus, in each PV-EL production node, for a given PV installed capacity (which is a decision variable), the HSC model knows the possible hydrogen production, which constrains the absorbed PV electricity by the EL per day (another decision variable). The grid electricity consumption to the EL per day is also a decision variable. The difference between a potential 24-hour operation of the electrolyser at nominal load and the available electricity from PV is the limit for grid electricity purchase. From these, hydrogen production per day is easily computed and enters the hydrogen mass balances of the model.

Figure A.2 illustrates the trends of the total electricity generated from PV and of the amount available to feed the electrolyser, as functions of the PV nominal capacity, in the PV-EL node of the province of Trapani (TP) as an example.

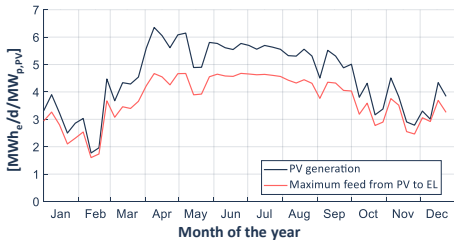


*Figure A.2. Year-long daily profiles of PV electricity generation in production node TP: total amount (blue line) and amount available to EL (orange line). The amount possibly absorbed by the EL is always larger (12 $MWh_{el}/d/MW_p$).*

## Appendix 2: GIS methodology

The two candidate transport networks implemented in the model are obtained by appropriately manipulating the shapefiles retrieved at the DIVA-GIS database [77]. In order to provide the transport networks as input

to the optimization model, the shapefiles are converted into directed graphs. In general, the road and natural gas shapefiles consist of *MultiLineString* geometries (i.e., a list of edges), and they may differ in terms of coordinate system and/or frame of reference. The shapefiles are first handled in the software QGIS, where they are standardised in terms of coordinate system, frame of reference, and maximum length of the geometries, and where the line vertices are extracted and exported to an additional shapefile. Then, the networks and vertices shapefiles are imported to MATLAB®, where they are converted into directed graphs exploiting the Mapping Toolbox and a set of dedicated functions. The graphs are completed with the addition of demand and production nodes. Each of them is connected to the nearest node on the graph through a straight line, and a detour factor is introduced to account for the fact that actual connections might be longer to comply with the territorial features of the area. In particular, detour factors of 1.3 [98] and 1.4 [45] are introduced for road and pipeline connections, respectively. To reduce the graphs dimension, redundant dead-end paths that do not terminate at neither production nor demand nodes are removed, thus preserving only the pathways that can actually be exploited in transport. Finally, the set of candidate intermediate storage nodes is identified for each graph through a random extraction among transit nodes, ensuring that they are evenly distributed.

## Appendix 3: Seasonality effects

Given that most of the regional hydrogen demand is supplied by RES-based production (see Section 6.1), the storage profiles would be expected to exhibit a strong seasonality. Figure A.3. shows the year-long evolution of the hydrogen storage content at an intermediate storage node (Figure A.3..a) and at a production node (Figure A.3..b), featuring installed capacities of 173 $t_{H2}$ and 43 $t_{H2}$, respectively. Such nodes are representative of the behaviour of the intermediate storage hubs and of the storage section within production facilities, respectively. Both consist of liquid hydrogen storage, since it is the only form in which intermediate hubs are installed and the only case in which the installed capacity at production is larger than the lower boundary. Indeed, in the proposed model formulation, hydrogen production nodes may include all conditioning modes and the corresponding storage forms, but in most cases the installed storage capacity corresponds to the lower boundary (i.e., 1-day equivalent of the conditioning capacity) and therefore it is impossible to spot seasonality by looking at the operational profiles.

As opposed to the expected behaviour, only the intermediate storage hub features an evident seasonal trend, whereas the storage section of the production facility is filled and emptied multiple times throughout the year.

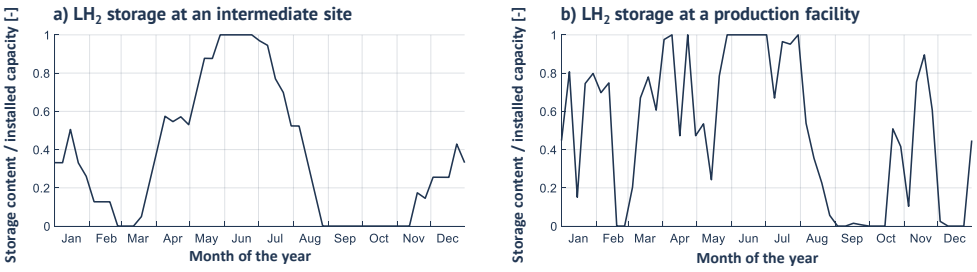


*Figure A.3. Year-long evolution of the hydrogen storage content at an LH2 intermediate storage site (a) and at a production facility (b).*

Such a behaviour is a consequence of many concurrent factors. First, the demand profiles of the mobility sector follow a seasonal trend in line with that of the solar radiation, thus reducing the need to store large quantities of hydrogen during summer to compensate the PV generation deficit in winter. In addition, flexible SMR-CCS production and the possibility to use grid electricity in PV-EL systems provide inexpensive alternatives to hydrogen storage to balance the fluctuations of the solar radiation. Another reason could be

the adoption of the typical day approach, which may lead to significant peaks and valleys in the storage profiles due to the repetition of inlet and outlet flows. A model run that avoids the day repetition and considers 365 time steps is performed to assess the impact of the typical day approach, considering a mono-modality application using pipeline delivery to preserve the model computational tractability. A representative production node is considered, and the evolution of its storage content is reported in Figure A.4.. Despite the absence of flow repetitions, the storage content still follows irregular profiles with frequent filling and emptying, indicating that the typical day approach is not responsible for this behaviour.

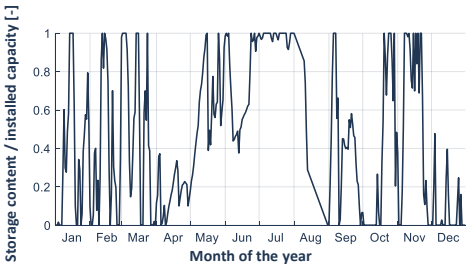


*Figure A.4. Year-long evolution of the hydrogen storage content at a production facility, in a mono-modality simulation over 365 time steps.*

Although all the abovementioned phenomena impact the results, the predominant reason behind the absence of seasonality in the evolution of the storage content at production nodes is the irregularity of the PV generation profiles themselves, which feature a stable profile during summer (May-September) and sudden peaks during the year (e.g., in January, March, and November). Comparing Figure A.3. and Figure A.5. (the dark blue line in Figure A.5. refers to the same production node), a correspondence between the peaks in PV generation and in the storage content emerges. To assess the consistency of the adopted data, which come from a punctual reference to one location within each province, they are compared against the regional aggregated PV generation historical time series [99] in Figure A.5.. Data are represented in terms of daily generation considering an average day per week, for a total of 52 typical days. As the figure shows, the provincial profiles and the regional aggregate follow a very similar trend, thus excluding errors introduced by the punctuality of the exploited profiles.

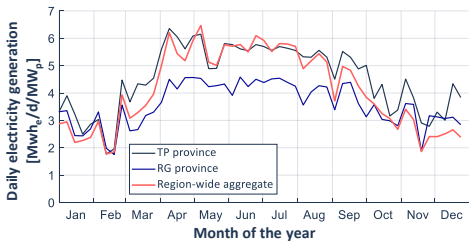


*Figure A.5. Comparison of the employed provincial PV generation profiles with the region-wide aggregated PV generation, considering an average day per week. Both data sets are referred to 2015.*

The upper boundary of the hydrogen storage capacity at production nodes might represent a further reason why seasonal effects are not observed at such nodes, since it may be too strict to fully absorb the peaks of PV-EL production during summer. However, such a limit is required to guarantee a reasonable land occupation of the storage section of production facilities, as they already occupy large areas due to the installation of PV fields. At any rate, the model allows the creation of large storage hubs at intermediate nodes, following the example of the natural gas infrastructure, in which storage is performed at strategic sites.

## Nomenclature

*Acronyms and abbreviations*

| | |
|---|---|
| BEV | Battery electric vehicle |
| CAPEX | Capital expenditure |
| CCS | Carbon capture and storage |
| CRF | Capital recovery factor |
| CT | Carbon tax |
| EL | Electrolysis |
| FCEV | Fuel cell electric vehicle |
| G | Gaseous hydrogen storage |
| GT | Compressed gaseous hydrogen truck transport |
| GP | Gaseous hydrogen pipeline transport |
| GDP | Gross domestic product |
| GIS | Geographic information system |
| HSC | Hydrogen supply chain |
| HRS | Hydrogen refuelling station |
| L | Liquid hydrogen storage |
| LCA | Life cycle assessment |
| LCOH | Levelized cost of hydrogen |
| LHV | Lower heating value |
| LIQ | Liquefaction |
| LOHC | Liquid organic hydrogen carrier |
| LRC | Lined rock cavern |
| LT | Liquid hydrogen truck transport |
| MILP | Mixed integer linear programming |
| O&M | Operation and maintenance |
| OPEX | Operational expenditure |
| P2H | Power-to-Hydrogen |
| PV | Photovoltaic |
| PV-EL | Integrated hydrogen production system composed of PV and EL |
| RD | Road delivery |
| RES | Renewable energy sources |
| SMR | Steam methane reforming |
| SMR-CCS | Steam methane reforming equipped with CCS |

*Subscripts and superscripts*

| | |
|---|---|
| *cnd* | Conditioning |
| *dem* | Demand |
| *edg* | Edge |
| *in* | Inlet flow |

| | |
|---|---|
| *nom* | Nominal |
| *out* | Outlet flow |
| *prd* | Production |

*Sets*

| | |
|---|---|
| $e \in E^m$ | Edges of the graph of transport modality $m$ |
| $m \in M$ | Available hydrogen transport modalities |
| $n \in N^m$ | Nodes of the graph of modality $m$ (i.e., $N^m = N_p \cup N_s^m \cup N_d \cup N_t^m$) |
| $n \in N_d$ | Hydrogen demand nodes |
| $n \in N_p$ | Candidate hydrogen production nodes |
| $n \in N_s^m$ | Candidate intermediate storage nodes of the graph of modality $m$ |
| $n \in N_t^m$ | Transit nodes of the graph of transport modality $m$ |
| $p \in P$ | Available hydrogen production technologies |
| $s \in S$ | Available hydrogen storage technologies |
| $t \in T$ | Time steps |

*Parameters*

| | |
|---|---|
| $\tilde{c}_E$ | Electricity purchase cost (€/$MWh_e$) |
| $\tilde{C}_{GP,max}$ | Upper boundary of pipeline capacity ($m^2$) |
| $\tilde{C}_{GP,min}$ | Lower boundary of pipeline capacity ($m^2$) |
| $\tilde{C}_{prd,max}^{n,p}$ | Upper boundary of production capacity for technology $p$ at node $n \in N_p$ ($t_{H2}$/d) |
| $\tilde{C}_{PV,max}^{n}$ | Upper boundary of PV capacity at node $n \in N_p$ ($MW_{nom}$) |
| $\tilde{c}_{RD}$ | Specific OPEX for road delivery (€/km) |
| $\tilde{C}_{s,dem,max}^{n,m}$ | Upper boundary of storage capacity at node $n \in N_d$ for modality $m$ ($t_{H2}$) |
| $\tilde{C}_{s,dem,min}^{n,m}$ | Lower boundary of storage capacity at node $n \in N_d$ for modality $m$ ($t_{H2}$) |
| $\tilde{c}_{tax}$ | Carbon tax (€/$t_{CO2}$) |
| $\tilde{C}_{truck}^{m}$ | Truck capacity for transport modality $m \in \{GT, LT\}$ ($t_{H2}$/truck) |
| $\widetilde{capex}_i$ | Specific capital cost of component $i$ (€/unit) |
| $\widetilde{capex}_{fix,i}$ | Intercept of the linear expression for the CAPEX of component $i$ (€) |
| $\widetilde{capex}_{var,i}$ | Slope of the linear expression for the CAPEX of component $i$ (€/unit) |
| $\widetilde{cons}_{cnd}^{m}$ | Conditioning specific consumption for modality $m$ ($kWh_e$/($t_{H2}$/d)) |
| $\widetilde{cons}_{EL}$ | Electrolysis specific consumption ($MWh_e$/$t_{H2}$) |
| $\tilde{e}_i$ | $CO_2$ emission factor of component $i$ ($t_{CO2}$/$MWh_e$ or $t_{CO2}$/$t_{H2}$) |
| $\tilde{f}_{conv}^{m}$ | Conversion factor for conditioning capacity (($t_{H2}$/d)/$kW_e$) |
| $\tilde{f}_{PV\text{-}EL}^{n,t}$ | Electricity fed to EL from PV per unit of PV capacity at node $n \in N_p$ and time step $t$ ($MWh_e$/d/$MW_{nom}$) |
| $\tilde{f}_{PV,tot}^{n,t}$ | Electricity generated per unit of PV capacity at node $n \in N_p$ and time step $t$ ($MWh_e$/d/$MW_{nom}$) |
| $\tilde{k}_{dem}^{m}$ | Fraction of daily demand required as storage content at the beginning of each time step for modality $m$ |
| $\tilde{k}_{max,prd}^{s}$ | Upper boundary of storage capacity at production nodes for technology $s$ (equivalent days of conditioning capacity) |

$\tilde{k}^{s}_{min,prd}$ Lower boundary of storage capacity at production nodes for technology $s$ (equivalent days of conditioning capacity)

$\tilde{l}^{e}$ Length of edge $e$ (km)

$\widetilde{N}_{td}$ Number of repetitions of each typical day (#)

$\widetilde{opex\%}_{O\&M_i}$ O&M cost, as percentage of CAPEX of component $i$ ($y^{-1}$)

$\tilde{p}_{E}$ Electricity sale price (€/$MWh_e$)

$\tilde{q}^{n,t}_{dem}$ Hydrogen demand at node $n$ and time step $t$ ($t_{H2}$/d)

$\tilde{r}_{PV\text{-}EL}$ Ratio between electrolysis and PV nominal capacities in the integrated PV-EL system

$\tilde{Y}^{m,n}$ Incidence matrix of the directed graph of the modality $m$, evaluated at node $n \in N^m$

$\widetilde{\Delta t}$ Time resolution (d)

$\tilde{\varepsilon}_{s}$ Fractional loss for storage technology $s$ ($d^{-1}$)

*Continuous variables*

$C^{n,m}_{cnd}$ Conditioning capacity for modality $m$ at node $n \in N_p \cup N^m_s \cup N_d$ ($kW_e$ or $t_{H2}$/d)

$C^{n}_{PV}$ PV capacity at node $n \in N_p$ ($MW_{nom}$)

$C^{n,p}_{prd}$ Hydrogen production capacity at node $n \in N_p$ for technology $p$ ($t_{H2}$/d)

$C^{e}_{GP}$ Pipeline capacity at edge $e \in E^{GP}$ ($m^2$)

$C^{n}_{s}$ Storage capacity at node $n \in N_p \cup N^m_s \cup N_d$ for technology $s \in \{GP, LT\}$ ($t_{H2}$)

$CAPEX_i$ Capital cost of component $i$ (€)

$COH_{avg}$ Average cost of hydrogen delivered at demand points (€/$kg_{H2}$)

$E^{n,t}_{grid}$ Electricity from grid to EL at node $n \in N_p$ and time step $t$ ($MWh_e$/d)

$E^{n,t}_{PV}$ Electricity from PV to EL at node $n \in N_p$ and time step $t$ ($MWh_e$/d)

$E^{n,t}_{PV,tot}$ Total electricity generated from PV at node $n \in N_p$ and time step $t$ ($MWh_e$/d)

$E^{n,t}_{sur}$ Surplus electricity from PV at node $n \in N_p$ and time step $t$ ($MWh_e$/d)

$FC_i$ Fixed annual operational cost of component $i$ (€/y)

$OPEX_i$ Operational cost of component $i$ (€/y)

$q^{n,t}_{in,s}$ Inlet hydrogen flow for storage technology $s$, at node $n \in N_p \cup N^m_s \cup N_d$ and time step $t$ ($t_{H2}$/d)

$q^{n,m,t}_{cnd}$ Conditioning hydrogen flow for modality $m$, at node $n \in N_p \cup N^m_s \cup N_d$ and time step $t$ ($t_{H2}$/d)

$q^{e,m,t}_{edg}$ Hydrogen flow on edge $e$, with transport modality $m$, at time step $t$ ($t_{H2}$/d)

$q^{e,m,t}_{edg,ABS}$ Absolute value of $q^{e,m,t}_{edg}$ for $m \in \{GT, LT\}$

$q^{n,t}_{out,s}$ Outlet hydrogen flow for storage technology $s$, at node $n \in N_p \cup N^m_s$ and time step $t$ ($t_{H2}$/d)

$q^{n,p,t}_{prd}$ Hydrogen production flow for technology $p$, at node $n \in N_p$ and time step $t$ ($t_{H2}$/d)

$Q^{n,t}_{s}$ Hydrogen storage content for technology $s$, at node $n \in N_p \cup N^m_s \cup N_d$ and time step $t$ ($t_{H2}$)

$VC_i$ Variable operational cost of component $i$ (€/y)

*Integer variables*

$C^{n}_{s}$ Storage capacity at node $n \in N_p \cup N_d$ for technology $s \in \{GT\}$ (# of trailers)

| | |
|---|---|
| $C^{n}_{trailer,LT}$ | Number of tank-equipped trailers at node $n \in N_p \cup N_s^{LT}$ (#) |
| $N^{e,m,t}_{truck}$ | Number of trucks in motion on edge $e \in E^m$ for modality $m \in \{GT, LT\}$ at time step $t$ (#/d) |

*Binary variables*

| | |
|---|---|
| $\xi^{n,m}$ | Use of transport modality $m$ at node $n \in N_d$ |
| $\chi^{e}_{GP}$ | Pipeline capacity at edge $e \in E^{GP}$ is within boundaries |
| $\chi^{n}_{LIQ}$ | Liquefaction capacity at node $n \in N_p$ is within boundaries |

## References


[1] European Commission, "Communication from the Commission to the European Parliament, the Council, the European Economic and Social Committee and the Committee of the Regions. A Roadmap for moving to a competitive low carbon economy in 2050," *COM(2011) 112*, 2011.

[2] P. Colbertaldo, S. B. Agustin, S. Campanari, and J. Brouwer, "Impact of hydrogen energy storage on California electric power system: Towards 100% renewable electricity," *Int. J. Hydrogen Energy*, vol. 44, no. 19, pp. 9558–9576, 2019.

[3] Fuel Cells and Hydrogen Joint Undertaking (FCH), "Hydrogen Roadmap Europe," 2019.

[4] Hydrogen Council, "Hydrogen Scaling Up," 2017.

[5] Hydrogen Council, "Policy Toolbox for Low Carbon and Renewable Hydrogen," 2021.

[6] Hydrogen Council, "Path to hydrogen competitiveness: a cost perspective," 2020.

[7] European Commission, "Communication from the Commission to the European parliament: A hydrogen strategy for a climate-neutral Europe," *COM(2020) 301*, 2020.

[8] Y. Ruf, M. Baum, T. Zorn, A. Menzel, and J. Rehberger, "Fuel Cell Hydrogen Trucks - Heavy-Duty's High Performance Green Solution," 2020.

[9] IEA, "Europe: key energy statistics." https://www.iea.org/regions/europe.

[10] J. Alazemi and J. Andrews, "Automotive hydrogen fuelling stations: An international review," *Renew. Sustain. Energy Rev.*, vol. 48, pp. 483–499, 2015.

[11] Gasworld, "SMR: Driving down costs in hydrogen production," 2014. https://www.gasworld.com/smr-driving-down-costs-in-hydrogen-production/2004183.article.

[12] IEAGHG, "Techno - Economic Evaluation of SMR Based Standalone (Merchant) Hydrogen Plant with CCS," 2017.

[13] IEA, "Hydrogen Production & Distribution," 2014.

[14] IEA, "The Future of Hydrogen," 2019.

[15] S. Campanari, P. Colbertaldo, and G. Guandalini, "Renewable power-to-hydrogen systems and sector coupling power-mobility," in *Energy, Environment and New Materials. Volume 1 – Hydrogen Production and Energy Transition*, M. Van De Voorde, Ed. De Gruyter, 2021.

[16] IRENA, "Hydrogen From Renewable Power," 2018.

[17] L. Welder, D. S. Ryberg, L. Kotzur, T. Grube, M. Robinius, and D. Stolten, "Spatio-temporal optimization of a future energy system for power-to-hydrogen applications in Germany," *Energy*, vol. 158, pp. 1130–1149, 2018.

[18] L. Li, H. Manier, and M. A. Manier, "Integrated optimization model for hydrogen supply chain network design and hydrogen fueling station planning," *Comput. Chem. Eng.*, vol. 134, 2020.

[19] IEA, "Technology Roadmap Hydrogen and Fuel Cells," 2015.

[20] DOE Hydrogen and Fuel Cell Technologies Office, "Fuel Cell Technologies Office Multi-Year Research, Development, and Demonstration Plan, 3.2 Hydrogen Delivery," 2015.

[21] H. Barthelemy, M. Weber, and F. Barbier, "Hydrogen storage: Recent improvements and industrial perspectives," *Int. J. Hydrogen Energy*, vol. 42, no. 11, pp. 7254–7262, 2017.

[22] Fuel Cells and Hydrogen 2 Joint Undertaking (FCH JU), "Addendum to the Multi-Annual Work Plan 2014-2020," 2018.

[23] HyUnder, "Assessment of the potential, the actors and relevant business cases for large scale and seasonal storage of renewable electricity by hydrogen underground storage in Europe. Overview on all Known Underground Storage Technologies for Hydrogen," 2013.

[24] D. G. Caglayan *et al.*, "Technical potential of salt caverns for hydrogen storage in Europe," *Int. J. Hydrogen Energy*, vol. 45, no. 11, pp. 6793–6805, 2020.

[25] T. Okuno, N. Wakabayashi, K. Niimi, Y. Kurihara, M. Iwano, and T. Komatsubara, "Advanced natural gas storage project and verification tests of lined rock cavern in Japan," *Intern. J. JCRM*, vol. 5, no. 2, pp. 95–102, 2009.

[26] J. Cihlar *et al.*, "ASSET Study on Hydrogen generation in Europe : Overview of costs and key benefits," 2021.

[27] JRC, "Assessment of Hydrogen Delivery Options," 2021.

[28] M. Moreno-Benito, P. Agnolucci, and L. G. Papageorgiou, "Towards a sustainable hydrogen economy: Optimisation-based framework for hydrogen infrastructure development," *Comput. Chem. Eng.*, vol. 102, pp. 110–127, 2017.

[29] M. Reuß, T. Grube, M. Robinius, P. Preuster, P. Wasserscheid, and D. Stolten, "Seasonal storage and alternative carriers: A flexible hydrogen supply chain model," *Appl. Energy*, vol. 200, pp. 290–302, 2017.

[30] C. Yang and J. Ogden, "Determining the lowest-cost hydrogen delivery mode," *Int. J. Hydrogen Energy*, vol. 32, no. 2, pp. 268–286, 2007.

[31] P. Colbertaldo, S. Cerniauskas, T. Grube, M. Robinius, D. Stolten, and S. Campanari, "Clean mobility infrastructure and sector integration in long-term energy scenarios: The case of Italy," *Renew. Sustain. Energy Rev.*, vol. 133, p. 110086, 2020.

[32] P. Preuster, C. Papp, and P. Wasserscheid, "Liquid organic hydrogen carriers (LOHCs): Toward a hydrogen-free hydrogen economy," *Acc. Chem. Res.*, vol. 50, no. 1, pp. 74–85, 2017.

[33] D. Teichmann, W. Arlt, and P. Wasserscheid, "Liquid Organic Hydrogen Carriers as an efficient vector for the transport and storage of renewable energy," *Int. J. Hydrogen Energy*, vol. 37, no. 23, pp. 18118–18132, 2012.

[34] Chiyoda Corporation, "SPERA Hydrogen." https://www.chiyodacorp.com/en/service/spera-hydrogen/ (accessed Apr. 27, 2021).

[35] Hydrogenious, "Hydrogenious." https://www.hydrogenious.net/ (accessed Apr. 27, 2021).

[36] N. Sabio, A. Kostin, G. Guillén-Gosálbez, and L. Jiménez, "Holistic minimization of the life cycle environmental impact of hydrogen infrastructures using multi-objective optimization and principal component analysis," *Int. J. Hydrogen Energy*, vol. 37, no. 6, pp. 5385–5405, 2012.

[37] Z. Li, D. Gao, L. Chang, P. Liu, and E. N. Pistikopoulos, "Hydrogen infrastructure design and optimization: A case study of China," *Int. J. Hydrogen Energy*, vol. 33, no. 20, pp. 5275–5286, 2008.

[38] A. Hugo, P. Rutter, S. Pistikopoulos, A. Amorelli, and G. Zoia, "Hydrogen infrastructure strategic planning using multi-objective optimization," *Int. J. Hydrogen Energy*, vol. 30, no. 15, pp. 1523–1534, 2005.

[39] G. S. Ogumerem, C. Kim, I. Kesisoglou, N. A. Diangelakis, and E. N. Pistikopoulos, "A multi-objective optimization for the design and operation of a hydrogen network for transportation fuel," *Chem. Eng. Res. Des.*, vol. 131, pp. 279–292, 2018.

[40] S. De-León Almaraz, C. Azzaro-Pantel, L. Montastruc, and M. Boix, "Deployment of a hydrogen supply chain by multi-objective/multi-period optimisation at regional and national scales," *Chem. Eng. Res. Des.*, vol. 104, pp. 11–31, 2015.

[41] G. Guillen-Gosalbez, F. D. Mele, and I. E. Grossman, "A Bi-Criterion Optimization Approach for the Design and Planning of Hydrogen Supply Chains for Vehicle Use," *AIChE J.*, vol. 56, no. 3, pp. 650–667, 2010.

[42] J. H. Han, J. H. Ryu, and I. B. Lee, "Multi-objective optimization design of hydrogen infrastructures simultaneously considering economic cost, safety and CO2 emission," *Chem. Eng. Res. Des.*, vol. 91, no. 8, pp. 1427–1439, 2013.

[43] J. O. Robles, C. Azzaro-Pantel, and A. Aguilar-Lasserre, "Optimization of a hydrogen supply chain network design under demand uncertainty by multi-objective genetic algorithms," *Comput. Chem. Eng.*, vol. 140, 2020.

[44] J. J. Brey, R. Brey, A. F. Carazo, I. Contreras, A. G. Hernández-Díaz, and V. Gallardo, "Designing a gradual transition to a hydrogen economy in Spain," *J. Power Sources*, vol. 159, no. 2, pp. 1231–1240, 2006.

[45] M. Reuß, T. Grube, M. Robinius, and D. Stolten, "A hydrogen supply chain with spatial resolution: Comparative analysis of infrastructure technologies in Germany," *Appl. Energy*, vol. 247, no. April, pp. 438–453, 2019.

[46] M. E. Demir and I. Dincer, "Cost assessment and evaluation of various hydrogen delivery scenarios," *Int. J. Hydrogen Energy*, vol. 43, no. 22, pp. 10420–10430, 2018.

[47] O. Tlili *et al.*, "Geospatial modelling of the hydrogen infrastructure in France in order to identify the most suited supply chains," *Int. J. Hydrogen Energy*, vol. 45, no. 4, pp. 3053–3072, 2020.

[48] C. Wulf *et al.*, "Life Cycle Assessment of hydrogen transport and distribution options," *J. Clean. Prod.*, vol. 199, pp. 431–443, 2018.

[49] A. Almansoori and N. Shah, "Design and operation of a future hydrogen supply chain: Snapshot model," *Chem. Eng. Res. Des.*, vol. 84, no. 6 A, pp. 423–438, 2006.

[50] S. Samsatli, I. Staffell, and N. J. Samsatli, "Optimal design and operation of integrated wind-hydrogen-electricity networks for decarbonising the domestic transport sector in Great Britain," *Int. J. Hydrogen Energy*, vol. 41, no. 1, pp. 447–475, 2016.

[51] A. Almansoori and N. Shah, "Design and operation of a future hydrogen supply chain: Multi-period model," *Int. J. Hydrogen Energy*, vol. 34, no. 19, pp. 7883–7897, 2009.

[52] M. Hoffmann, J. Priesmann, L. Nolting, A. Praktiknjo, L. Kotzur, and D. Stolten, "Typical periods or typical time steps? A multi-model analysis to determine the optimal temporal aggregation for energy system models," *Appl. Energy*, vol. 304, no. October, p. 117825, 2021.

[53] S. Baufumé *et al.*, "GIS-based scenario calculations for a nationwide German hydrogen pipeline infrastructure," *Int. J. Hydrogen Energy*, vol. 38, no. 10, pp. 3813–3829, 2013.

[54] N. Johnson, C. Yang, and J. Ogden, "A GIS-based assessment of coal-based hydrogen infrastructure deployment in the state of Ohio," *Int. J. Hydrogen Energy*, vol. 33, no. 20, pp. 5287–5303, 2008.

[55] A. Almansoori and A. Betancourt-Torcat, "Design of optimization model for a hydrogen supply chain under emission constraints - A case study of Germany," *Energy*, vol. 111, pp. 414–429, 2016.

[56] Y. Huang, Y. Fan, and N. Johnson, "Multistage System Planning for Hydrogen Production and Distribution," *Networks Spat. Econ.*, vol. 10, no. 4, pp. 455–472, 2010.

[57] A. Ochoa Bique, L. K. K. Maia, F. La Mantia, D. Manca, and E. Zondervan, "Balancing costs, safety and CO2 emissions in the design of hydrogen supply chains," *Comput. Chem. Eng.*, vol. 129, 2019.

[58] M. Ball, M. Wietschel, and O. Rentz, "Integration of a hydrogen economy into the German energy system: an optimising modelling approach," *Int. J. Hydrogen Energy*, vol. 32, no. 10–11, pp. 1355–1368, 2007.

[59] C. Yang and J. M. Ogden, "Renewable and low carbon hydrogen for California-Modeling the long term evolution of fuel infrastructure using a quasi-spatial TIMES model," *Int. J. Hydrogen Energy*, vol. 38, no. 11, pp. 4250–4265, 2013.

[60] P. Agnolucci, O. Akgul, W. McDowall, and L. G. Papageorgiou, "The importance of economies of scale, transport costs and demand patterns in optimising hydrogen fuelling infrastructure: An exploration with SHIPMod (Spatial hydrogen infrastructure planning model)," *Int. J. Hydrogen Energy*, vol. 38, no. 26, pp. 11189–11201, 2013.

[61] J. Kim, Y. Lee, and I. Moon, "Optimization of a hydrogen supply chain under demand uncertainty," *Int. J. Hydrogen Energy*, vol. 33, no. 18, pp. 4715–4729, 2008.

[62] H. T. Ingason, H. Pall Ingolfsson, and P. Jensson, "Optimizing site selection for hydrogen production in Iceland," *Int. J. Hydrogen Energy*, vol. 33, no. 14, pp. 3632–3643, 2008.

[63] M. Dayhim, M. A. Jafari, and M. Mazurek, "Planning sustainable hydrogen supply chain infrastructure with uncertain demand," *Int. J. Hydrogen Energy*, vol. 39, no. 13, pp. 6789–6801, 2014.

[64] S. Hwangbo, I. B. Lee, and J. Han, "Mathematical model to optimize design of integrated utility supply network and future global hydrogen supply network under demand uncertainty," *Appl. Energy*, vol. 195, pp. 257–267, 2017.

[65] W. Won, H. Kwon, J. H. Han, and J. Kim, "Design and operation of renewable energy sources based hydrogen supply system: Technology integration and optimization," *Renew. Energy*, vol. 103, pp. 226–238, 2017.

[66] H. Talebian, O. E. Herrera, and W. Mérida, "Spatial and temporal optimization of hydrogen fuel supply chain for light duty passenger vehicles in British Columbia," *Int. J. Hydrogen Energy*, vol. 44, no. 47, pp. 25939–25956, 2019.

[67] N. Strachan, N. Balta-Ozkan, D. Joffe, K. McGeevor, and N. Hughes, "Soft-linking energy systems and GIS models to investigate spatial hydrogen infrastructure development in a low-carbon UK energy system," *Int. J. Hydrogen Energy*, vol. 34, no. 2, pp. 642–657, 2009.

[68] S. Cerniauskas, A. Jose Chavez Junco, T. Grube, M. Robinius, and D. Stolten, "Options of natural gas pipeline reassignment for hydrogen: Cost assessment for a Germany case study," *Int. J. Hydrogen Energy*, vol. 45, no. 21, pp. 12095–12107, 2020.

[69] J. H. Han, J. H. Ryu, and I. B. Lee, "Modeling the operation of hydrogen supply networks considering facility

location," *Int. J. Hydrogen Energy*, vol. 37, no. 6, pp. 5328–5346, 2012.

[70] ESRI, "ESRI Shapefile Technical Description," 1998.

[71] L. Guo, R. Hou, Y. Liu, C. Wang, and H. Lu, "A novel typical day selection method for the robust planning of stand-alone wind-photovoltaic-diesel-battery microgrid," *Appl. Energy*, vol. 263, no. January, p. 114606, 2020.

[72] M. Zatti *et al.*, "k-MILP: A novel clustering approach to select typical and extreme days for multi-energy systems design optimization," *Energy*, vol. 181, pp. 1051–1063, 2019.

[73] L. Kotzur, P. Markewitz, M. Robinius, and D. Stolten, "Time series aggregation for energy system design: Modeling seasonal storage," *Appl. Energy*, vol. 213, no. January, pp. 123–135, 2018.

[74] G. L. Nemhauser and L. A. Wolsey, *Integer and Combinatorial Optimization*. New York: John Wiley & Sons, Incorporated, 1988.

[75] Mobilità Idrogeno Italia, "Piano Nazionale di Sviluppo," 2019.

[76] P. Colbertaldo, "Power-to-hydrogen for long-term power and transport sector integration," Politecnico di Milano, 2019.

[77] DIVA-GIS, "DIVA-GIS: spatial data by country." https://www.diva-gis.org/gdata.

[78] ENTSOG, "ENTSOG: the European natural gas network." https://entsog.eu/sites/default/files/2019-10/ENTSOG_CAP_2019_A0_1189x841_FULL_400.pdf.

[79] Il Sole 24 Ore, "Le raffinerie e l'indotto arrancano," 2014. https://www.infodata.ilsole24ore.com/2014/07/31/le-raffinerie-e-lindotto-arrancano/.

[80] European Commission, "Eurostat." https://ec.europa.eu/eurostat/home.

[81] United States Department of Labor, "U.S. Bureau of Labor Statistics." https://www.bls.gov/.

[82] Ministero dell'Ambiente e della Tutela del Territorio e del Mare, Ministero dello Sviluppo Economico, Ministero delle Infrastrutture e dei Trasporti, and Ministero delle Politiche agricole Alimentari e Forestali, "Strategia Italiana Di Lungo Termine Sulla Riduzione Delle Emissioni Dei Gas a Effetto Serra," 2021.

[83] ISPRA, "Fattori emissione produzione e consumo elettricità," 2018. http://www.sinanet.isprambiente.it/it/sia-ispra/serie-storiche-emissioni/fattori-di-emissione-per-la-produzione-ed-il-consumo-di-energia-elettrica-in-italia/at_download/file.

[84] IEA, "Net Zero by 2050," Paris, 2021.

[85] P. Colbertaldo, G. Guandalini, G. Lozza, and S. Campanari, "Sizing of integrated solar photovoltaic and electrolysis systems for clean hydrogen production," in *EFC2019 European Fuel Cell Technology & Applications - Piero Lunghi Conference EFC2019*, 2019, pp. 2019–2020.

[86] P. Bolat and C. Thiel, "Hydrogen supply chain architecture for bottom-up energy systems models. Part 2: Techno-economic inputs for hydrogen production pathways," *Int. J. Hydrogen Energy*, vol. 39, no. 17, pp. 8898–8925, 2014.

[87] IRENA, "Future of Solar Photovoltaic: Deployment, investment, technology, grid integration and socio-economic aspects (A Global Energy Transformation: paper)," Abu Dahbi, 2019.

[88] E. Crespi, P. Colbertaldo, G. Guandalini, and S. Campanari, "Design of hybrid power-to-power systems for continuous clean PV-based energy supply," *Int. J. Hydrogen Energy*, vol. 46, no. 26, pp. 13691–13708, 2021.

[89] W. Zappa, M. Junginger, and M. van den Broek, "Is a 100% renewable European power system feasible by 2050?," *Appl. Energy*, vol. 233–234, no. November 2018, pp. 1027–1050, 2019.

[90] Gestore Mercati Energetici (GME), "Dati storici MGP 2020," 2020. https://www.mercatoelettrico.org/It/download/DatiStorici.aspx.

[91] Eurostat, "Electricity prices for non-household consumers - bi-annual data (from 2007 onwards)." https://ec.europa.eu/eurostat/web/energy/data/database.

[92] E. Talpacci *et al.*, "Effect of cascade storage system topology on the cooling energy consumption in fueling stations for hydrogen vehicles," *Int. J. Hydrogen Energy*, vol. 43, no. 12, pp. 6256–6265, 2018.

[93] Terna, "Terna: statistics 2019," 2019. https://www.terna.it/it/sistema-elettrico/statistiche/pubblicazioni-statistiche.

[94] Terna SpA, "Industrial plan 2021-2025," 2020.

[95] Snam SpA, "2020-2024 Strategic Plan." https://www.snam.it/en/Investor_Relations/Strategy.

[96] The European House - Ambrosetti and Snam, "H2 Italy 2050," 2020.

[97] A. Arcos-Vargas, F. Nuñez, and R. Román-Collado, "Short-term effects of PV integration on global welfare and CO2 emissions. An application to the Iberian electricity market," *Energy*, vol. 200, 2020.

[98] M. Reuß, P. Dimos, A. Léon, T. Grube, M. Robinius, and D. Stolten, "Hydrogen road transport analysis in the energy system: A case study for germany through 2050," *Energies*, vol. 14, no. 11, pp. 1–17, 2021.

[99] ENTSO-E, "Actual Generation per Production Type," 2015. https://transparency.entsoe.eu/generation/r2/actualGenerationPerProductionType/show.